Available online at www.sciencedirect.com
SCIENCE DIRECT®
International Journal of Thermal Sciences 45 (2006) 237–256
International Journal of Thermal Sciences
www.elsevier.com/locate/ijts

# Preparation, measurement and analysis of the microstructure of evaporator surfaces

Andrea Luke *

*Institut für Thermodynamik, Universität Hannover, Callinstr. 36, 30167 Hannover, Germany*

Received 5 August 2004; received in revised form 23 March 2005; accepted 23 March 2005
Available online 15 November 2005

**Abstract**

The processes of the phase change in boiling occur at the solid–liquid interface by heat transfer from a solid heating surface to the boiling liquid. The characteristic features of the heating surfaces are therefore of great interest to optimize the design of evaporators. The microstructure with all its peaks and cavities influences directly the wetting and rewetting conditions of the heated surface by the boiling liquid and hence bubble formation and heat transfer. The heating elements of various subprojects within the research group working on fundamentals in boiling heat transfer are different in form and size (e.g. plates and tubes). Their micro- and macrostructure are characterized quantitatively with regard to the cavities offered to nucleation. The surfaces of the heating elements of varying materials (copper, copper alloys, steel and different metal layers) are emery ground or sandblasted resulting in a deterministic microstructure or a stochastic one. The surfaces are investigated by a three-dimensional contactless roughness measurement technique combining the stylus technique with the near field acoustic microscopy. The method opens the possibility to obtain results according to standard for practical applications and delivers detailed informations about the three-dimensional shape of each cavity within the surface investigated on the other side. The analysis of the microstructure implies the total number of cavities, their local and size distribution calculated by the method of the envelope area.


*Keywords:* Pool boiling; Nucleation sites; Surface roughness; Microstructure; Evaporator surfaces

## 1. Introduction

Many engineering problems involve boiling heat transfer. The processes of the phase change occur at the solid–liquid interface by heat transfer from a solid heating surface to the boiling liquid. The main advantages of boiling systems are that large heat transfer rates may be achieved with small temperature differences. The optimal design of the evaporators recently becomes more and more important because of the increasing miniaturization to save energy and to conserve the natural resources. Empirical correlations such as those of Gorenflo [1] in the VDI-Heat Atlas or of Cooper [2] are no longer sufficient for the design of the compact heat exchanger. These calculation methods are based on more or less exact heat transfer measurements and it is often not possible to extrapolate them beyond the range of the correlated measured data, e.g. for higher pressures, heat fluxes, superheat, or other liquids, because fundamental data are missing, e.g. of bubble formation. Therefore, the phase change processes should be better understood presently.

The long-term aim in the design of evaporators is to find prediction methods deduced from the real physical phenomena of the growing and departing bubbles and their activation on the heating surface. A detailed analysis of the microstructure of the evaporator surface, its wetting behaviour and the bubble formation of differently treated surfaces are as important as measurements of the heat transfer from these surfaces to the boiling liquid. The wide scatter within the experimental data of the heat transfer measurements in literature may be mainly explained by the large differences between the surface structures of the varying heating elements. A systematic knowledge of the microstructure of the heating surface and the bubble formation and motion on and along the superheated surface is still insufficient and hardly considered in empirical correlations. They should be interpreted if the phenomena of boiling heat transfer are linked to the local evaporating process. The final aim

* Tel.: +49 0511 762 2277; fax: +49 0511 762 3857.
*E-mail address:* luke@ift.uni-hannover.de (A. Luke).

1290-0729/$ – see front matter © 2005 Published by Elsevier SAS.
doi:10.1016/j.ijthermalsci.2005.03.018

**Nomenclature**

| | | |
|---|---|---|
| $A$ | area | $m^2$ |
| $d_p$ | particle size | mm |
| $D$ | tube diameter | m |
| $g$ | density distribution | |
| $h$ | probability function | |
| $m$ | exponent | |
| $N$ | number of potential nucleation sites | |
| $N/A_{max}$ | total number of cavities | $mm^{-2}$ |
| $p$ | pressure | Pa, bar |
| $P_0$ | largest cavity | µm |
| $P_a$, $P_q$, $P_p$, $P_{pm}$, $P_t$, $P_z$ | standardized roughness parameter acc. to DIN EN ISO 4287 for two-dimensional profiles without cut-off | µm |
| $P5^*$ | roughness parameter characterizing a cavity | µm |
| $R_a$, $R_q$, $R_p$, $R_{pm}$, $R_t$, $R_z$ | standardized roughness parameter acc. to DIN EN ISO 4287 for filtered two-dimensional profiles | µm |
| $R_B$ | roller radius for creating the envelope areas | µm |
| $R_{p,old}$ | Glättungstiefe acc. to DIN 4262, 08.1960 | µm |
| $S_a$, $S_q$, $S_p$, $S_t$, $S_z$ | roughness parameter acc. to DIN EN ISO 4287 adapted for topographies acc. to Stout et al. [34] | µm |
| $s_{pot}$ | nearest distance between neighbouring potential nucleation sites | µm |
| $x$ | gauge length | mm |
| $x$, $y$, $z$ | coordinates of the topographies | µm |

*Greek symbols*

| | | |
|---|---|---|
| $\alpha$ | heat transfer coefficient | $W{\cdot}m^{-2}{\cdot}K^{-1}$ |
| $\gamma_1$ | skewness | |
| $\gamma_2$ | excess | |
| $\lambda_c$ | cut-off | mm |
| $\sigma$ | standard deviation | |

of these efforts is to predict the heat transfer in boiling on industrial surfaces. They show a large variety of roughness and structures due to the manufacturing process. This effects a large difference in the number of active nucleation sites and consequently in heat transfer.

The formation and growth of bubbles in particularly favourable sites of the heating surfaces is one of the main mechanisms of heat transfer in boiling, thus the superheat in the heating wall and the liquid is locally reduced. Colder liquid flows into the superheated boundary layer after bubble departure and the liquid will be superheated in turn. The formation and growth of the bubbles on the heating surface evoke turbulences and by this way a well mixed fluid. The effect of the microscopic and macroscopic form of the heating surface on the surface-fluid system is multifaceted: the microscopic structure (= roughness) with its elevations and cavities influences directly the wetting and dewetting of the heating surface by the fluid and consequently bubble formation and heat transfer. The macroscopic form of the heating surface and its arrangement in the evaporator intensifies or impedes the movement of the fluid and the up-streaming bubbles. This creates additional convective effects which locally influence bubble formation and heat transfer in different ways.

The cavities in technically rough heating surfaces are potential nucleation sites depending on the thermophysical liquid properties and the operating parameters, such as superheat, heat flux, and saturation pressure. At small superheats of the heating surface and low saturation pressures bubble formation is promoted by a few number of large cavities. At higher superheats and high pressures more and smaller cavities become active, e.g. within the flanks of the large cavities.

The paper deals with the characterization of the micro- and macrostructure of different heating surfaces. This implies a detailed and precise analysis of the topography in addition to standardized measurement techniques. The heating elements have been used for investigations of heat transfer and bubble formation or vapour/liquid distribution on the surface by other research groups interior the joint project on fundamentals of boiling heat transfer of this special issue. The surfaces are similar to the industrial ones but prepared by special reproducible processes in the laboratory. Their microstructure is treated by emery grinding or sandblasting by the same procedure. Different materials, forms and sizes of the heating surfaces are used: copper, CuNi and stainless steel tubes ($D = 15$ mm [3,4], $D = 24.0$–$25.4$ mm [5,6]), copper plates ($15 \times 200$ mm [7]), and tubes coated galvanically by gold [8], and plates sputtered with layers of different material [9]. Macro cavities have been prepared by a rolling process similar to the industrial processes [10,11]. Changes of the surface microstructure by fouling or destruction effects can be correlated with changes of the boiling processes [10,12,13].

## 2. Preparation and measurement procedure

The typical technical rough surface structure of evaporators results from a large variety of manufacturing processes: e.g. the single tubes of a bundle are drawn, special macrostructures on these tubes to enhance the heat transfer are rolled, and the thin plates of a plate heat exchanger are milled. The surfaces are cleaned preoperationally by sandblasting or by chemical means. The number, form and size of the cavities and their local distribution on such surfaces differ in a wide range. All these preparation methods affect consequently large variations in activation of bubble nucleation sites and in heat transfer. Reproducible processes are developed for the preparation of heating surfaces in the laboratory similar to the industrial surfaces. The preparation methods shall simulate a large range of industrial processes.

The measurement methods have to allow an exact analysis of the particular original heating surfaces independent of their size or form. The results shall not only consider manufacturing

items but they shall offer the possibility to correlate the surface structure of the heating element with the local bubble formation and wall superheat investigated by experiment using the same heating element after the surface analysis.

### 2.1. Preparation of evaporator surfaces

Some of the heating elements used in literature show a surface structure resulting from the industrial manufacturing processes: drawn wires [16] or tubes [17], rolled tubes with enhanced surfaces [11,18], milled thin plates [19]. Procedures to prepare a uniform structure of various heater geometries with different dimensions have been developed recently to achieve equally distributed potential nucleation sites independent of form and size of the heating element, e.g. plates, tubes or special enhanced surfaces. The surfaces are carefully polished before the final preparation to guarantee the same basis structure. The final microstructures of the heating surfaces are either emery ground or sandblasted, representing a drawn or milled surface or a blast cleaned one in technical application, respectively. The emery grinding, sandblasting or rolling procedure is described in detail elsewhere [13,20]. In the following, the treatment parameters are shortly discussed. The surface structures are classified into the deterministic structures with orderly separated grooves, examples are emery ground, milled or rolled surfaces, and the stochastically structures with statistically distributed peaks and cavities, e.g. the sandblasted surface.

*Emery grinding procedure.* A large number of tubes and plates for research purpose are emery ground because of the simple preparation method. Complex preparatory measures in order to protect the sensitive measuring and heating sensors arranged below the surface are not necessary. However, the grinding parameters are often not mentioned in literature or are not exactly reproducible (e.g. the manually treated surfaces in Table 1). A highly reproducible method for axially grinding, especially of tubes (horizontally installed in the evaporator [21]) of different sizes is developed, for details of the mechanical facility see [20]. The method have been transferred even for plates or thin sheets [22]. The parameters of treatment are

- the grade of the emery cloth (size and form of the grain per area),
- the contact pressure of the cloth on the surface,
- the number of the motions of the cloth over the surface.

The cloth is installed with exactly adjusted contact force on a slide guided parallel to the tube axis. The result is a metallically reflecting surface with regular grooves. A contact pressure of $p_{con} \approx 0.05$ N·mm$^{-2}$ of 400 grade emery cloth effects on copper a mean roughness of $R_a \approx 0.4$ μm normal to the grooves. This is the reference value of the surface roughness of the empirical correlation of the VDI-Heat Atlas [1], which is mainly based on emery ground copper surfaces. The mean roughness of a mild steel tube is only half the value for copper using the same grinding parameters. A survey of the grinding parameters of different emery ground surfaces used within the joint research project is given in Table 1.

A surface worked irregularly with constant changes in the grinding direction has a nondirectional structure with grooves interrupted several times by others [10]. Different roughness may be achieved by systematic changes of the grinding parameters, particularly the granulation of the emery cloth, ranging from very smooth, polished surfaces with $P_a = 0.03$ μm up to rough surfaces with 1 μm (in the case of softer materials such as copper). The polishing procedure using a very high grade of emery cloth, e.g. #1000 or #4000, is preferable for very sensible surfaces, as in the case of a horizontal copper heater sputtered with a gold layer, see Table 1, where micro thermocouples are embedded with a distance of 3.6 μm to the surface [9].

*Sandblasting procedure.* The mechanical facility for reproducible sandblasting includes a tube injector which is shifted over the surface by a motorized device in a sandblasting cabin, for details see [20]. An uniform granular structure all over the surface is achieved independently of the form and macrostructure (for wires [25] or complex macrostructures as special

Table 1
Survey of the grinding parameters of the heating surfaces

| Heater element Material | Grinding parameters | | | Mean Roughness | Ref.[a] |
|---|---|---|---|---|---|
| | Granulation | Contact pressure | Number of motions | | |
| tube, $D = 15$ mm copper | #400 | 0.05 N·mm$^{-2}$ | 20 axial | $P_a = 0.41$ μm | R: [13] H: [3]; B: [3] |
| sample tube, $D = 15$ mm stainless steel | #400 | 0.05 N·mm$^{-2}$ | 20 axial | $P_a = 0.17$ μm | R: [3] |
| plate, $D = 18.2$ mm copper with Ni-layer | polished manually #1000 | – | – no direction | $P_a = 0.052$ μm | R: [10] H: [24]; B: [24] |
| plate, $D = 35.0$ mm copper with Ni-layer | polished manually #1000 | – | – no direction | $P_a = 0.12$ μm | R: [10] H: [12]; B: [12] |
| plate, $D = 35.0$ mm copper with Au-layer | polished manually #4000 | – | – no direction | $P_a = 0.11$ μm | R: this paper H: [9]; B: [23] |

[a] R: roughness results; H: investigations of heat transfer in boiling, and B: investigations of bubble formation in boiling and of vapour/liquid distribution in transition boiling.

finned tubes, or enhanced surfaces [6,26]). The parameters of sandblasting are

- the size, form and material of the sandblasting particles,
- the pressure,
- the distance between injector tube and the heating surface,
- the number of the motions of the injector tube over the surface.

Mean roughness of $R_a = 0.2$ μm up to 10 μm is achieved by sandblasting rather than by emery grinding [15]. The heating surfaces of different form and size investigated by the project partners are mainly fine sandblasted, see the survey in Table 2. Material effects can be easily excluded using the same sandblasting parameters such as corundum grain of particle sizes $d_p = 0.02$–$0.03$ mm with a low pressure of $p_L = 1.5$ bar. Almost identical standardized roughness parameters are obtained for copper and copper alloys, and some gold and stainless steel layers, see Table 2. The procedure provides reproducibly the same microstructure within the statistical scatter after several removals of the original fine sandblasted surface e.g. of the copper tube ($D = 25.4$ mm). Higher pressures, e.g. $p_L = 5$

Table 2
Survey of the sandblasting parameters of the heating surfaces

| Heater element Material | Sandblasting parameters | | | Mean Roughness | Ref.[a] |
|---|---|---|---|---|---|
| | Size, form and material of the grains | Pressure $p_L$ [bar] | Number of motions | | |
| tube, $D = 25.4$ mm copper 1st preparation | fine sandblasted pure corundum $d_p = 20$–$30$ μm | 1.5 | 2 | $P_a = 0.25$ μm | R: [13] H: [5,14]; B: [29,30] |
| tube, $D = 25.4$ mm copper 2nd preparation after removal of the macro cavities | fine sandblasted pure corundum $d_p = 20$–$30$ μm | 1.5 | 2 | $P_a = 0.24$ μm | R: [13] H: [5,14]; B: [29,30] |
| tube, $D = 24.0$ mm CuNI | fine sandblasted pure corundum $d_p = 20$–$30$ μm | 1.5 | 2 | $P_a = 0.24$ μm | R: [13] H: [5]; B: 5 |
| tube, $D = 24.0$ mm CuNI | fine sandblasted pure corundum $d_p = 20$–$30$ μm | 1.5 | 2 | $P_a = 0.21$ μm | R: [10] |
| tube, $D = 15.0$ mm copper with Au layer | fine sandblasted pure corundum $d_p = 20$–$30$ μm | 1.5 | 2 | $P_a = 0.30$ μm | R: [10] H: [8]; B: [8] |
| tube, $D = 15.0$ mm stainless steel | fine sandblasted pure corundum $d_p = 20$–$30$ μm | 1.5 | 2 | $P_a = 0.14$ μm | R: this paper H: [4]; B: [4] |
| tube, $D = 15.0$ mm stainless steel with gold layer | fine sandblasted pure corundum $d_p = 20$–$30$ μm | 1.5 | 2 | $P_a = 0.26$ μm | R: this paper H: [27]; B: [27] |
| plate, $D = 35.0$ mm copper with stainless steel layer | fine sandblasted pure corundum $d_p = 20$–$30$ μm | 1.5 | 2 | $P_a = 0.20$ μm | R: [10] H: [12]; B: [12] |
| plate, $15 \times 200$ mm copper | fine sandblasted pure corundum $d_p = 20$–$30$ μm | 5.0 | 2 | $P_a = 0.44$ μm | R: [13] H: [28]; B: [28] |
| plate, $15 \times 200$ mm copper | fine sandblasted pure corundum $d_p = 20$–$30$ μm | 1.5 | 2 | $P_a = 0.26$ μm | R: [10] H: [7]; B: [7] |
| tube, $D = 25.0$ mm copper | fine sandblasted pure corundum $d_p = 20$–$30$ μm | 3.0 | 2 | $P_a = 0.57$ μm | R: this paper |
| | then medium sandblasted pure corundum $d_p = 50$–$80$ μm | 1.5 | 2 | | |

The distance between nozzle and surface is set constant to 210 mm.

[a] R: roughness results; H: investigations of heat transfer in boiling, and B: investigations of bubble formation in boiling and of vapour/liquid distribution in transition boiling.

bar, result in a mean standardized roughness of the reference value $R_a = 0.4$ μm like the emery ground copper surfaces, although the structure is totally different, see the copper plate [27] in Table 2. The disadvantages of the sandblasting procedure with high pressures are deposits of the sandblasting material in the heating surface, especially on soft materials such as gold and copper and that a complicated protection for the sensitive measurement and control technique of the heating elements is required.

The structure and roughness of sandblasted surfaces varies manifold and reentrant cavities are provided by different treatments succeeding each other, so that one surface superimposes the other, e.g. by first fine then medium sandblasting or vice versa. The result is a surface microstructure similar to industrial manufactured surfaces, see the fine and then medium sandblasted copper tube in Table 2 with $D = 25.0$ mm. Here, the outer diameter of the copper tube is reduced because of the several preparations and removals of the different micro- and macrostructures. The microstructure is rougher than those of other surfaces. Sandblasting with a mixture of different fractions of grains (e.g. fine corundum grains of $d_p = 20 \ldots 30$ μm mixed with a wider particle fraction $d_p = 50 \ldots 80$ μm) causes also a wider distribution of cavity sizes than using one single fraction. More large cavities and less smaller cavities are obtained than on a surface prepared with the succeeding method.

*Rolling procedure.* The macro cavities of industrially manufactured (finned) enhancement tubes are polyform and complex [17,18]. Even conventional fin tubes depending on the rolling procedure show different mean roughness values on the top, flank and the ground of the fins. The new generation of enhanced tubes [17] should not be sandblasted to obtain a uniform microstructure, because then the grains are entrapped in the cavities and finally influence the boiling mechanism in an unpredictable way. The rolled macrostructure shows a variety of narrow channels and cavities. The original activation process of the bubble nuclei cannot be observed by optical means [29, 30]. New treatment methods for special macro cavities are required for an interpretation of the real enhancement effects, i.e. for the description of the local mechanism in bubble formation and heat transfer [5,6,11].

Copper and CuNi tubes with a defined basic microstructure are rolled after the heat transfer measurement by means of industrial procedures in two steps: once rolled results in the "secondary" structure with open cavities regularly distributed in azimuthal and axial direction (see also Chapter 3). The macro cavities show comparatively simple shapes of ca. $120 \times 250 \times 50$ μm$^3$ [5,10,11,15]. The previous microstructure (e.g. fine sandblasted or fine-medium sandblasted, see Table 2) is preserved during the rolling procedure. A succeeding plain rolling treatment flattens the material between the macro cavities into them, so that the main structure provides reentrant cavities [11]. The aperture of the cavities can be varied by the rolling parameters (such as the tool geometry or the contact pressure). The previous microstructure is now destroyed and is similar to a drawn copper microstructure [22]. A range with the original microstructure without impressed macrostructure separates the different sorts of macro cavities.

*Coatings.* Heating surfaces are coated with a metal layer such as copper, nickel, stainless steel or gold

- to locate the measurement technique of the wall temperature directly beneath the surface [9,12,23,24],
- to investigate the influence of the material on the heat transfer [8],
- to protect the wall against corrosion effects.

After the coating procedure the surface is treated by the mechanical methods (sandblasting, emery grinding and polishing) described above, see Tables 1 and 2.

### 2.2. Measurement technique for evaporator surfaces

The relationship between the surface topography with all its elevations, peaks and cavities, and its influence on boiling heat transfer has been partially investigated using two-dimensional (2D)-surface analysis. This analysis limits our idea of the microstructure of technical rough surfaces, especially of anisotropic ones. A full understanding of the links between surface topography and evaporating process can only be realized with a three-dimensional (3D) surface characterization. The following methods for measuring the geometrical characteristics of the microstructure (roughness) and macrostructure are established in connection with boiling heat transfer, cf. Fig. 1:

- stylus based instruments: conventionally contact scanning systems [20], contactless scanning by optical methods based on focus detection [20] or by methods using ultrasound [10,13,22,31],
- optical based systems: focus detection, e.g. confocal method, defect of focus method, interferometry, e.g. holographic interferometry,
- scanning microscopic based systems: electron microscopy (Scanning Electron Microscope = SEM), electron probe microscopy (Atomic Force Microscope = AFM, and Scanning Tunnelling Microscope = STM).

The best-known methods for a quantitative description of the micro- and macrostructure of technically rough surfaces up to a magnitude of ±800 μm are the stylus-based measurement instruments. The method is easy to apply without complicated preparation of the test object. The main boundary conditions and the results in form of roughness parameters are standardized especially for manufacturing reasons (DIN EN ISO 3274). The method has been used and improved for decades for heating surfaces [20,31,32]. The resolution limits imposed by the geometry of the stylus tips are clearly visible. Especially narrow and deep grooves in the surface structure are not registered, thus leading to a deviation of the measurable differences in height and inclination angles, see the sketch true to scale in Fig. 2.

Surface measuring methods operating with laser beams deliver a better resolution, since the beam diameter does not

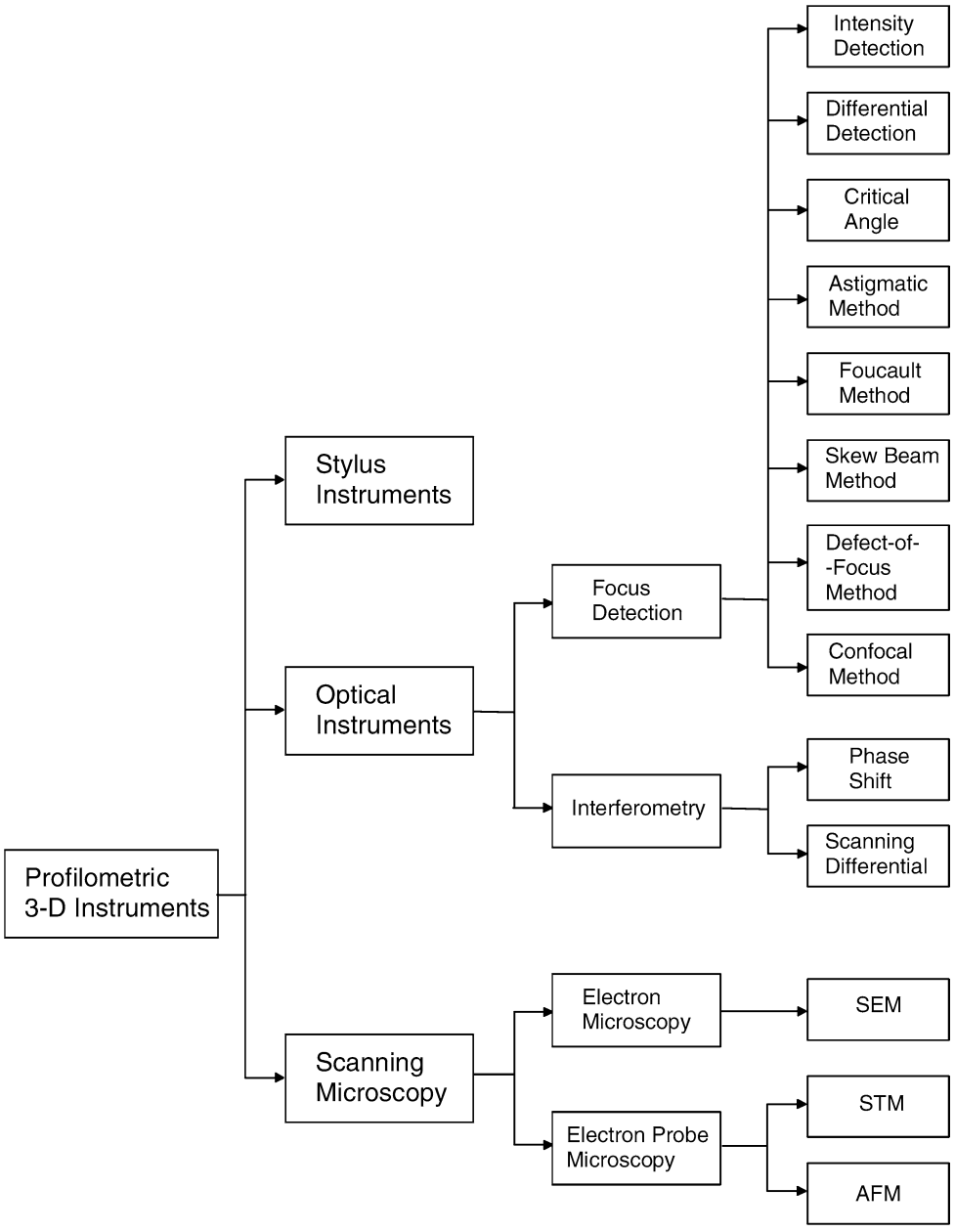


Fig. 1. Review of different profilometric three-dimensional measurement instruments.

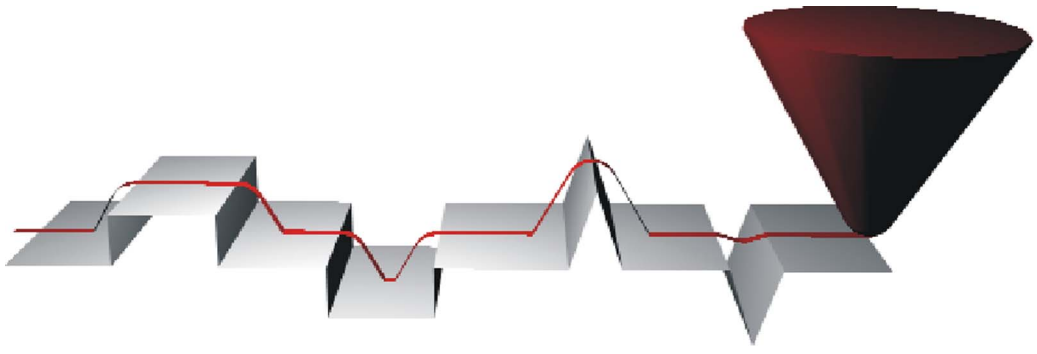

Fig. 2. Misinterpretation of the measured profile by the geometry of the standard stylus tip with a cone angle of 90° (full-scale).

exceed 1 μm [20]. Optical based methods are widely applied mainly for highly reflecting and/or smooth surfaces (as e.g. surfaces of compact discs). They are often not suitable for technical rough surfaces with optical diffuse sandblasted surfaces [20]. The resolution achieved by scanning microscopic based systems (SEM, AFM) is far better, located either within the range of an electron beam diameter (10 nm) or limited by the subsequent electronics. Still, the methods based on SEM procedures used today for surface structure measurements deliver only two-dimensional images, and are therefore not particularly well-suited for the quantitative characterization of heated surfaces. Additionally, heating surfaces of a technical scale, e.g. long tubes with special features for temperature measurement, heating facilities among others, do not fit into the chamber of a scanning electron microscope, high-resolution images with a great depth of focus can only be recorded on sample surfaces until now. Reentrant cavities of the size of some microns, favourable for the activation of nucleation sites, cannot be measured by none of these methods without destroying the heating element. Removing the top layer of the surface by emery grinding combined with repeated microscope photographs is problematic.

New developments of the contactless stylus system from the near field-acoustic microscopy are applied to combine the advantages of high-resolution AFM with those of the conventional stylus instrument [33]. This method uses a tuning fork swinging quartz, as found in quartz clocks with frequencies of more than 30 000 Hz. A diamond with a defined tip radius like those of the contact stylus is attached to the tuning fork. The resonance characteristics of the oscillator are changed by the hydrodynamic friction effect when approaching the surface with a pick-up tip (distance 1 to max. 10 μm). This is caused by the compressibility of the air layer when moving the tip towards the solid surface. The radius of the diamond tip of the ultrasonic stylus is only restricted by the manufacturing process and has values of 1 μm which is the same size as the focus mark of optical systems and is thereby smaller than that of conventional contact systems (Fa. Hommelwerke, Schwenningen, Germany). The movements of the tip in vertical $z$-direction correspond to the surface roughness as in the case of a conventional contact stylus instrument but without the risk of damaging the original surface by creating new cavities or grooves. This method allows the investigation of both very soft surfaces (biological samples, textile tissues) as well as very hard ones (e.g. diamond layers) without any abrasion. Although the stylus tip is much smaller than a conventional one, see the measured profile of a cavity element on a once rolled and subsequently smoothed tube in Fig. 3, the restricting geometry of the stylus tip has still to be considered.

One scan in $x$-direction by the stylus tip represents a conventional roughness profile as in Fig. 4, top left with the standard parameters according to DIN EN ISO 4287 (10.98). The conventional gauge length of $x = 0.5$ mm of the profiles investigated within this paper is shorter than standardized to obtain a higher resolution. Topographies are measured on an area of $0.5 \times 0.5$ mm$^2$ due to the long measuring time. Precise forward feeds in $y$-direction, normal to the $x$-direction of the single profile, provide single scans with a very small distance of $\Delta y = 0.5$ μm in minimum, see Fig. 4, right. At the end of each two-dimensional $x, z$-measurement the stylus is shifted from the surface during the reverse motion. The new profile recording is started after a latency for vibration reducing of the measurement chain. Evaluation programmes enable the isometrical (left) and photorealistical (right) representation of the topography with more than 1000 single scans in Fig. 4, right bottom (as example serves an emery ground copper tube with $D = 15$ mm and $P_a = 0.41$ μm, see Table 1). Differently treated surfaces (emery ground, sandblasted, drawn, milled, rolled) have been investigated recently by this method [22]. The inaccuracies of the measuring chains result in at most 0.6% of the standardized roughness parameters (linear advance and stylus system with 2 nm).

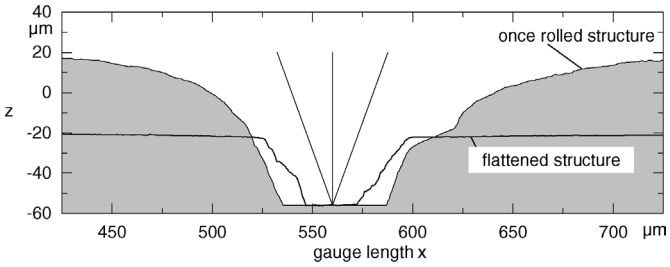


Fig. 3. Misinterpretation of the measured profile of a rolled and then flattened macrostructure with the ultrasonic stylus tip (full-scale).

Several measurements with $\Delta y = 25$ μm of two-dimensional profiles are carried out over all thermocouples within the heating surface with the highest resolution $\Delta z = 1$ nm (for smooth surfaces without rolled macrostructure) and $\Delta x = 11$ nm. Topographies are investigated with a similar resolution in both directions $\Delta x = \Delta y = 0.5$ μm over selected locations of area for bubble formation, considering the long measuring time.

Summing up, it may be said that topographies of the smooth surfaces as treated by fine and medium sandblasting, emery grinding or milling and drawing have the size of $0.5 \times 0.5$ mm$^2$, rolled surfaces are extended up to 1 mm $\times$ 10.0 mm with lower resolution in $y$-direction $\Delta y = 10$ μm. In some few cases, the total topography could not be entirely investigated because of exterior interferences. Then, the area investigated is reduced in $y$-direction.

## 3. Characterization of evaporator surfaces

### 3.1. Standardized roughness parameters

The idea of technical rough surfaces, e.g. an axially emery ground copper tube, is mainly influenced by the two-dimensional profiles with the typical enlargement as in Fig. 4. Quantitative results for the differently treated heated surfaces are in the first instance given by mean values like the standardized roughness parameters resulting from the statistical analysis of the 2-D surface data of the surface profiles. They are suitable to describe the quality of a surface in a manufacturing processes, and they are simple to determine. The standardized integral roughness parameters referring to the depth are also used to consider the

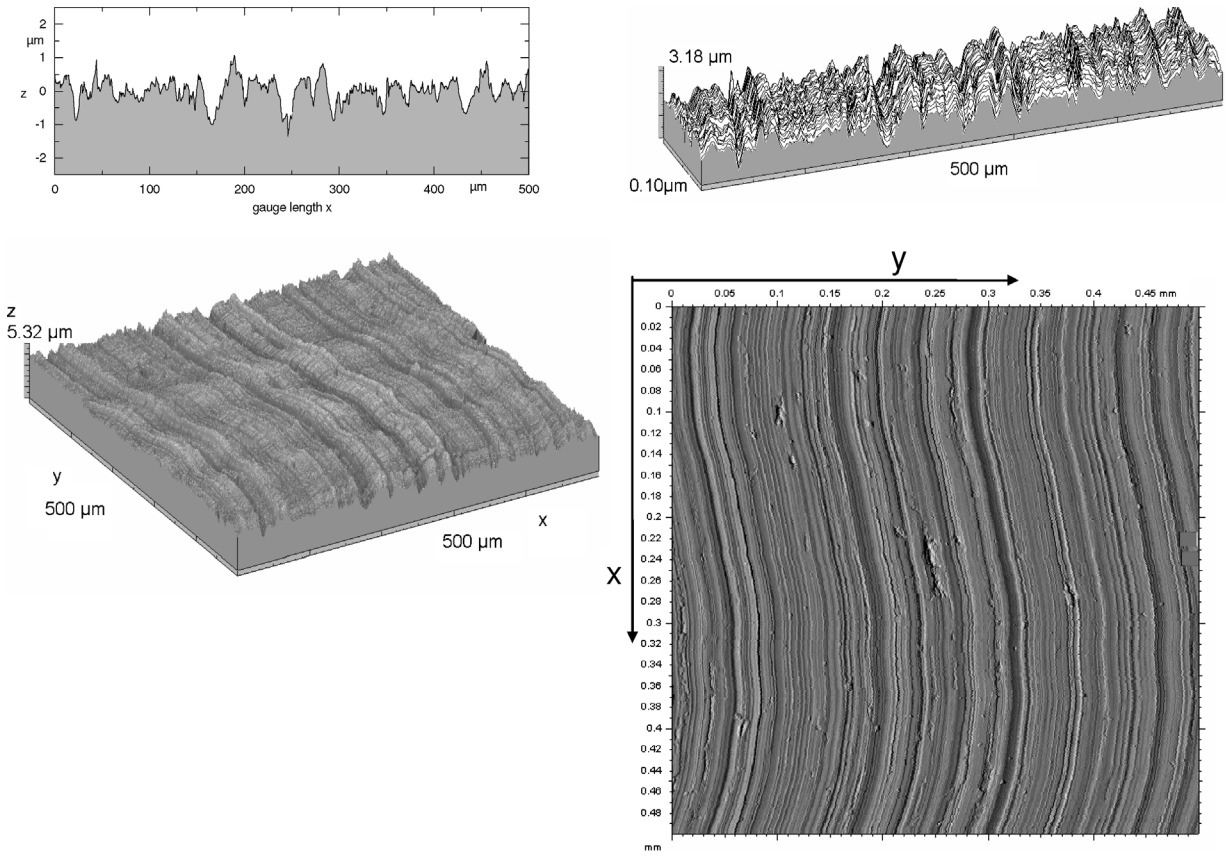


Fig. 4. A typical profile (enlargement $z/x = 36$) and the first single scans providing the isometric (left) and photorealistic (right) representation of the topography of an emery ground copper tube, cf. also Table 1.

effect of surface roughness on heat transfer in boiling by the empirical correlations, e.g. $R_a$ by Gorenflo [1] and $R_{p,\mathrm{old}}$ by Cooper [2].

The standardized roughness parameters $P$ and $R$ describe the deviation of the measured 2-dimensional profile (= 2-D analysis) from the reference (= ideal) line $z = 0$. $P$ is related to the "primary profile" according to DIN EN ISO 4287 (10.98), i.e. the profile without cut-off ($\lambda = \infty$). The parameter $R$ considers the standard cut-off. In this case the filtered profile is used. The new results of differently treated heating surfaces will be represented in form of $P$-values to avoid misinterpretation effects by filtering. The definition of the roughness parameters is analogous to the former DIN 4762 and 4768 (05.90), $P_a$ and $P_q$ are integral mean parameters corresponding to $R_a$, $R_q$, $P_p$ and $P_t$ are singular parameters, $P_z$ and $P_{\mathrm{pm}}$ are the average values of five equal parts of the gauge length, their definition is given in Table 3. $P_p$ or $R_p$, respectively, is not the same "Glättungstiefe" as used by Stephan [35] and by Cooper [2] in their correlation for characterizing the surface roughness. The "former Glättungstiefe" $R_{p,\mathrm{old}}$ was defined as the averaged distance between the profile and its envelope curve produced by a roller radius of $R_B = 25$ mm according to DIN 4762 (08.60). Modern digital stylus instruments consider only the new definition.

Statistical analysis of 2-D surface data and their distributions have produced informations relating to the character of manufactured surfaces. However, the inevitable conclusion from such analysis is that there is a fundamental limitation in using 2-D analysis in an attempt to describe a 3-D surface. Obviously, if the surface structure is anisotropic, very significant variations will be obtained especially if profiles are traced in differing directions relative to the predominant one. A coherent approach to 3-D surface topography analysis is proposed: The deviation from a flat plate, the topography, is defined by the parameter $S_i$ according to Stout et al. [34]. Many of the 2-D parameters that have evolved since the onset of digital surface analysis have equivalent counterparts in 3-D characterization, see Table 3. For example, in 2-D analysis the average roughness parameter, $P_a$, is a measure of "the absolute deviation of the profile ordinate heights from the mean line". This parameter can be defined in 3-D analysis as $S_a$ "the absolute deviation of the profile height ordinates from the mean plane". The singular peaks and cavities are described by $S_t$ and $S_p$, see Table 3. However, there is no equivalent definition in the case of $P_{\mathrm{pm}}$.

### 3.2. Statistical analysis of cavities

The determination of the standard roughness parameters is the conventional method to characterize quantitatively the surface microstructure. The difficulties of using these mean values have been discussed intensively in the past. For instance, the total variation between the highest and the lowest deviation from the median line of the profile expressed by similar $P_z$ or $P_t$ values are obviously not appropriate to characterize cavity sizes. Focussing on each single cavity will be important in fu-

Table 3
Definition of standard roughness parameters

| Two-dimensional (DIN EN ISO 4287 10.98): related to the profile | Three-dimensional (Stout et al. [34]) related to the topography |
|---|---|
| $P_a$ arithmetic mean roughness height<br>$P_a = \frac{1}{x} \cdot \int_0^x \lvert z(x) \rvert \, \mathrm{d}x$ | $S_a$ arithmetic mean roughness height<br>$S_a = \frac{1}{xy} \sum_x \sum_y \lvert z_{x,y} \rvert$ |
| $P_q$ quadratic mean roughness height<br>$P_q = \sqrt{1/x \cdot \int_0^x z^2(x) \, \mathrm{d}x}$ | $S_q$ quadratic mean roughness height<br>$S_q = \sqrt{\frac{1}{xy} \sum_x \sum_y z_{x,y}^2}$ |
| $P_t$: roughness height: vertical difference between the highest and the deepest point within the profile | $S_t$: total height of the surface vertical difference between the highest and the deepest point within the topography |
| $P_p$: "Glättungstiefe" vertical difference between the highest peak and the meridian line | $S_p$ max. peak of the surface: vertical difference between the highest peak and the mean ideal plane surface of the topography |
| $P_z$: mean roughness height<br>$P_Z = \frac{1}{5} \cdot \sum_{i=1}^{5} Z_i$ | $S_z$: mean depth of the surface: mean value of the five highest peaks and the deepest cavities within a scatter of $3 \times 3$ |
| $P_{\mathrm{pm}}$: mean "Glättungstiefe"<br>$P_{\mathrm{pm}} = \frac{1}{5} \cdot \sum_{i=1}^{5} P_{pi}$ | |

ture to obtain the missing link to the local bubble formation and superheat of the wall, because they are apt to be potential nucleation sites which are activated depending on the thermophysical properties of the boiling liquid and on the operation parameters as superheat and saturation pressure.

The calculation method of the envelope curve or area, respectively, created by a variable roller radius $R_B$ is used for the quantitative analysis of the measured two-dimensional profiles or three-dimensional topographies. The input data for modelling are only the $x$, $y$, $z$-data of the topography measurements. The method is deduced from a proposal of Stephan [35] to apply the former definition of the Glättungstiefe $R_{p,\mathrm{old}}$ representing the vapour/gas amount trapped between the envelope and the measured (real, technical rough) surface. Smaller roller radii immerse deeper into the profile/topography to identify more and smaller cavities, and few and larger cavities are determined by the larger roller radii. A cavity is defined as succeeding contact points of the envelope curve with the profile (in this case the cavities are treated as a projection of the real three-dimensional cavities in idealized shape [20]) and as the three nearest contact points of the envelope area with the topography (describing the real polymorphic form of the cavities). The geometric properties of the cavities within the measured surface microstructure are summarized in various roughness parameters, e.g. the mouth width of the cavity, the mean depth and to refer the cavities to the critical radius of a bubble nucleus, $P5^*$ is defined as the third root of the volume of the largest spherical bubble activated possibly at the deepest point of the cavity between the profile and the envelope curve/area [30], see Fig. 5.

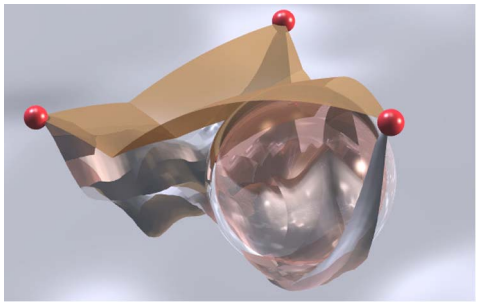

Fig. 5. Definition of a cavity and of the roughness parameter $P5^*$.

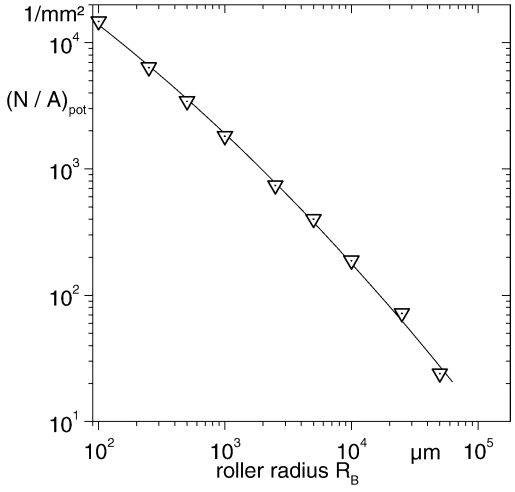


Fig. 6. Total number of potential sites $N/A_{\mathrm{pot}}$ for a fine sandblasted copper tube as function of the roller radius $R_B$.

### 3.3. Review of recently published results

The results in form of the standardized roughness parameters (mean value and standard deviation) of the heated surfaces published recently are summarized in Table 4. The 3-D parameters are supplied now. Examples of the topographies and profiles of these surfaces are published [10,13,22]. The fine sandblasted procedure serves as "reference" for the research group to obtain nearly the same mean surface roughness ($P_a$-value) and surface structure independent of form, size and material of the heating element. The main advantage is that this procedure could be realized on surfaces with very sensible measurement technique with embedded micro-thermocouples within the copper plate coated with a stainless steel layer [9]. The disadvantage is that the surface structure is smoother and more regular than industrial manufactured surfaces or as the emery ground surface with the reference $P_a$-value of 0.4 µm, cf. the copper tube of $D = 15$ mm in Table 1.

The fine sandblasting treatment of all surfaces results in a granular surface microstructure with an average arithmetic mean roughness height of $P_a \approx 0.25$ µm $\pm 0.05$ µm. The roughness parameters tend to lower values for harder materials as stainless steel, and to higher values for the softer gold layer on the copper tube, see Table 4. The values of $S_a$ are higher than $P_a$ in the case of the fine sandblasted surfaces. The singular parameters $S_t$ and $S_p$ are higher because the single events

Table 4
Review of recently published roughness parameters of heating elements acc. to DIN EN ISO 4287 (10.98) with the gauge length of $x = 0.5$ mm, without cut-off ($\lambda_c = \infty$)

| Heater element, Material, Treatment | | $P_a$ [µm] | $P_q$ [µm] | $P_p$ [µm] | $P_{pm}$ [µm] | $P_t$ [µm] | $P_z$ [µm] | Runs | Ref. |
|---|---|---|---|---|---|---|---|---|---|
| tube, $D = 25.4$ mm | average | 0.25 | 0.32 | 1.03 | 0.79 | 2.16 | 1.65 | 266 | [13] |
| copper, fine sandblasted | $\sigma$ | 0.02 | 0.03 | 0.19 | 0.10 | 0.31 | 1.17 | | |
| | $S_i$ [a] | 0.29 | 0.36 | 1.82 | | 3.73 | 1.91 | 1 | |
| tube, $D = 24.0$ mm | average | 0.24 | 0.31 | 1.04 | 0.78 | 2.02 | 1.55 | 220 | [13] |
| CuNi, fine sandblasted | $\sigma$ | 0.02 | 0.03 | 0.24 | 0.13 | 0.18 | 0.31 | | |
| | $S_i$ [a] | 0.27 | 0.34 | 2.26 | | 4.02 | 3.52 | 1 | |
| tube, $D = 24.0$ mm | average | 0.21 | 0.27 | 0.96 | 0.71 | 1.90 | 1.45 | 350 | [10] |
| CuNi, fine sandblasted | $\sigma$ | 0.02 | 0.02 | 0.24 | 0.09 | 0.34 | 0.14 | | |
| | $S_i$ [a] | 0.26 | 0.32 | 1.54 | | 3.30 | 3.05 | 1 | |
| tube, $D = 15.0$ mm | average | 0.30 | 0.38 | 1.16 | 0.90 | 2.51 | 1.94 | 45 | [10] |
| copper with a plated | $\sigma$ | 0.03 | 0.04 | 0.35 | 0.14 | 0.38 | 0.19 | | |
| Au-layer, fine sandblasted | $S_i$ [a] | 0.34 | 0.43 | 1.93 | | 4.34 | 4.11 | 1 | |
| plate, $D = 35$ mm | average | 0.20 | 0.27 | 1.18 | 0.80 | 1.82 | 1.33 | 100 | [10] |
| copper with a plated | $\sigma$ | 0.02 | 0.03 | 0.33 | 0.14 | 0.36 | 0.17 | | |
| stainless steel layer, fine sandblasted | $S_i$ [a] | 0.24 | 0.32 | 2.82 | | 4.03 | 3.42 | 2 | |
| plate, $15 \times 200$ mm | average | 0.26 | 0.33 | 0.96 | 0.75 | 2.19 | 1.69 | 92 | [10] |
| copper, fine sandblasted | $\sigma$ | 0.02 | 0.03 | 1.18 | 0.08 | 0.32 | 0.14 | | |
| | $S_i$ [a] | 0.23 | 0.33 | 1.74 | | 3.98 | 3.58 | 1 | |
| plate, $15 \times 200$ mm | average | 0.44 | 0.55 | 1.48 | 1.03 | 2.99 | 2.12 | 114 | [13] |
| copper, fine sandblasted | $\sigma$ | 0.07 | 0.09 | 0.29 | 0.16 | 0.50 | 0.28 | | |
| ($p_L = 5$ bar) | $S_i$ [a] | 0.45 | 0.58 | 3.02 | | 5.95 | 5.30 | 3 | |
| tube, $D = 15$ mm | average | 0.41 | 0.51 | 1.44 | 1.10 | 3.18 | 2.29 | 44 | [13] |
| copper, emery ground | $\sigma$ | 0.10 | 0.11 | 0.48 | 0.29 | 0.71 | 0.47 | | |
| | $S_i$ [a] | 0.40 | 0.50 | 2.31 | | 5.85 | 5.36 | 3 | |
| plate, $D = 18,2$ mm | average | 0.05 | 0.07 | 0.19 | 0.14 | 0.53 | 0.36 | 45 | [13] |
| copper with a plated Ni-layer, | $\sigma$ | 0.01 | 0.01 | 0.04 | 0.02 | 0.13 | 0.04 | | |
| polished manually | $S_i$ [a] | 0.14 | 0.17 | 0.93 | | 1.88 | 1.39 | 2 | |
| plate, $D = 35$ mm | average | 0.12 | 0.16 | 0.76 | 0.50 | 1.37 | 0.95 | 90 | [10] |
| copper with a plated Ni-layer, | $\sigma$ | 0.01 | 0.01 | 0.21 | 0.09 | 0.24 | 0.11 | | |
| polished manually | $S_i$ [a] | 0.16 | 0.20 | 2.59 | | 4.11 | 2.76 | 1 | |

[a] $S_i(S_a, S_q, S_p, S_t, S_z)$ correspond to the two-dimensional, see Table 3, the number of runs is the number of investigated topographies.

increase on the total area. Sandblasting with higher pressure results in $P_a$-values near the emery ground copper tube, even near the reference value of the VDI-Heat Atlas [1], see the result of a copper plate using $p_L = 5$ bar in Table 4. The results of the emery ground copper tube represent the roughness normal to the direction of the grooves. Along the grooves the values are smaller [15]. The two manually polished Ni-plated copper plates differ more than the half between $P_a = 0.05 \ldots 0.12$ µm due to the non-reproducible treatment method, see Table 4.

A statistical analysis is carried out for the fine sandblasted copper tube with $P_a = 0.25$ µm [29,30], because the local superheat and the bubble formation are investigated coincidently [14,22,29,30]. The total number of potential nucleation sites related to 1 mm$^2$ are represented as function of the roller radius in Fig. 6. The number of cavities increases with decreasing roller radii $R_B$ in a similar way the number of active nucleation sites increase with decreasing critical radii of the nuclei or with increasing saturation pressure and superheat. As each cavity within the fine sandblasted microstructure of the copper tube has different forms and sizes described by the parameter $P5^*$, the size distribution is calculated for different roller radii for all cavities found in the area investigated by the stylus instrument ($A = 0.5 \times 0.5$ mm$^2$). The cumulative size distribution of $P5^*$ can be represented by a modified RRS-function (= Rosin, Rammler, Sperling-function) for the dimensionless number $N$ of cavities on a given surface area (e.g. 1 mm$^2$)

$$\frac{N}{A} = \int_{P_{\max}}^{P} g(P)\,\mathrm{d}P = \left(\frac{N}{A}\right)_{\max} \exp\left[-\ln\left(\frac{N}{A}\right)_{\max}\left(\frac{P}{P_o}\right)^m\right] \quad (1)$$

The characteristic parameters of the distribution are the largest value $P_0$ (= the largest cavity), and the total number $(N/A)_{\max}$ of cavities found on the whole measured area, and the exponent m, characterizing the slope of the distribution. The analysis of the fine sandblasted surface results in the cumulative

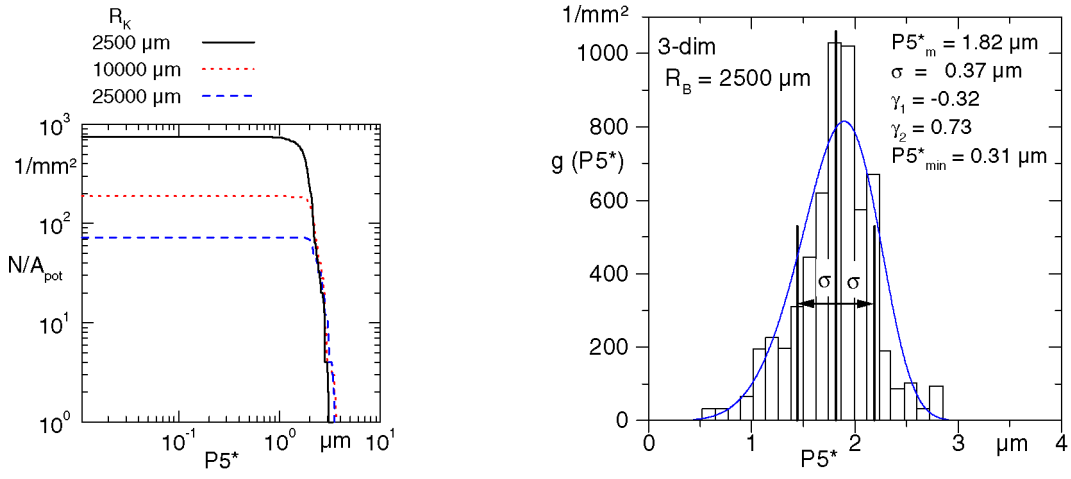


Fig. 7. Cumulative size distribution of the parameter $P5^*$ (left) and density distribution of the three-dimensional analysis for $R_B = 2500$ µm for the fine sandblasted surface with $P_a = 0.25$ µm.

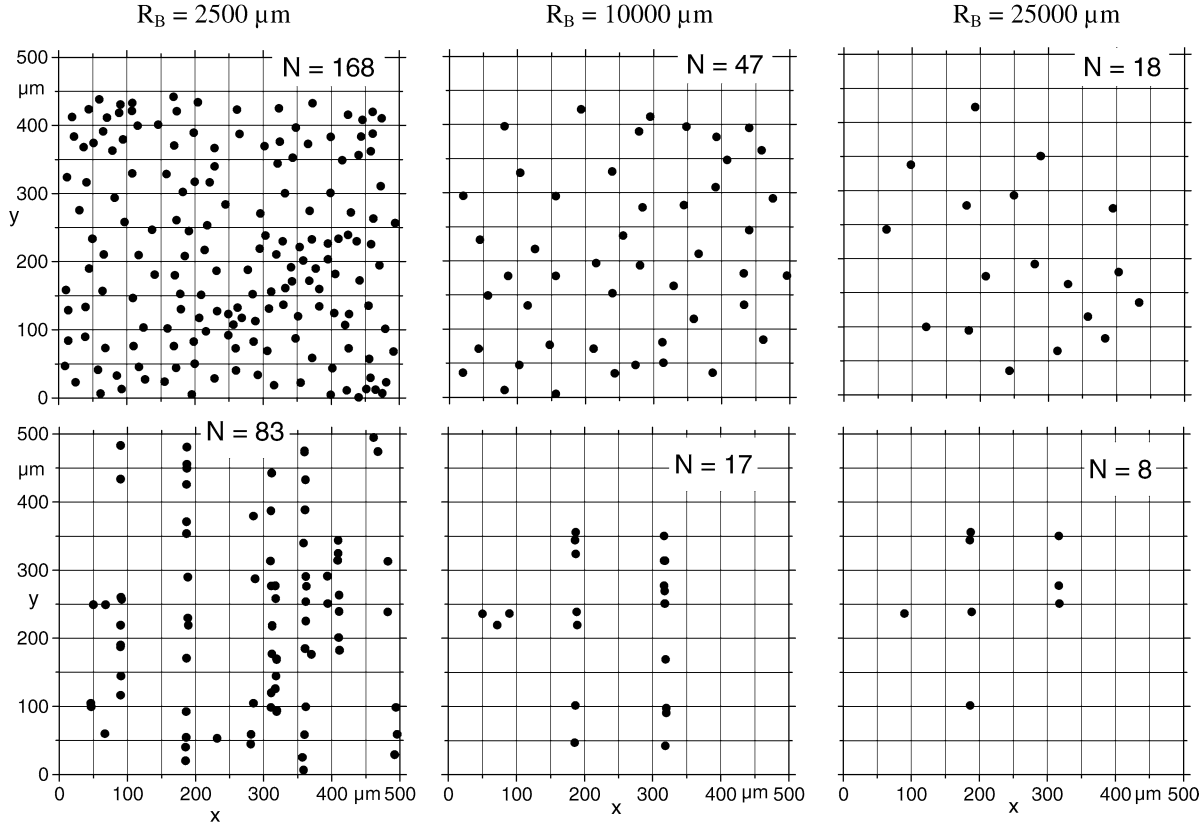


Fig. 8. Cavity location map for different roller radii for the fine sandblasted copper tube (top, $D = 25.4$ mm, $P_a = 0.25$ µm) and an emery ground tube (bottom) [15].

distribution of $P5^*$ for three different roller radii in Fig. 7, left. The largest cavity for the example ($P5_0^* \approx 3.4$ µm) is nearly independent of the three roller radii, but the total number of small cavities is ten times larger with increasing $R_B$. Larger cavities cannot be found on smooth surfaces as the fine sandblasted one.

The probability density $g(P)$ is the derivative of the cumulative size distribution and has the form of a Weibull distribution extended by $(N/A)_{\max}$. $g(P)$ specifies the number of cavities within the size interval between $|P|$ and $|P + \mathrm{d}P|$:

$$g(P) = \frac{\mathrm{d}}{\mathrm{d}P}\left(\frac{N}{A}\right) = \left(\frac{N}{A}\right)_{\max} \ln\left(\frac{N}{A}\right)_{\max} \frac{m}{P_0^m} P^{m-1} \exp\left[-\ln\left(\frac{N}{A}\right)_{\max}\left(\frac{P}{P_0}\right)^m\right] \quad (2)$$

Fig. 7, right, shows the Weibull distribution belonging to the roller radius $R_B = 2500$ µm in Fig. 7, left, for the fine sandblasted copper tube. The sizes of the cavities have a very narrow distribution, the scatter is only $\sigma = \pm 0.37$ µm to an average

value of $P5^*_m = 1.82$ µm, and they are distributed uniformly, excess $\gamma_2$ and skewness $\gamma_1$ are almost zero.

The potential nucleation sites are distributed statistically on the area investigated by the different roller radii for the fine sandblasted surface, see Fig. 8, top. The analysis of the possible interaction of the nucleation processes between each other is represented by means of the density distribution of the distances of the nearest adjacent potential sites $s_{\text{pot}}$ in Fig. 9. The

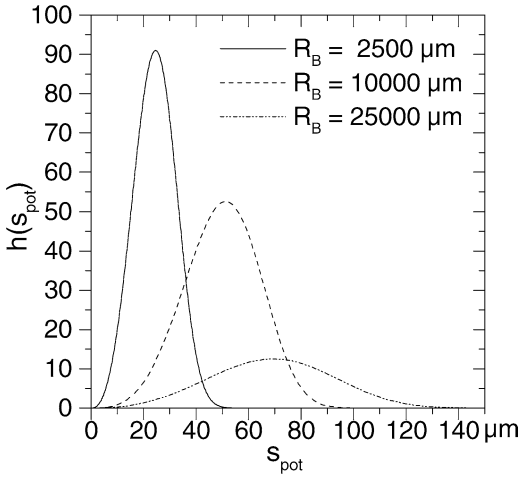


Fig. 9. Probability distribution of the distances of the nearest adjacent potential nucleation sites $s_{\text{pot}}$ for different roller radii for the fine sandblasted surface of Fig. 8, top.

modified Weibull distribution according to Eq. (2) for the different roller radii of the fine sandblasted surface show distances relatively small in comparison to those of active nucleation sites ($s_{\text{act},m} = 78$ µm) [10]. The cavity location maps are typical for the fine sandblasted surfaces, while those of axially emery ground tubes have totally different local distributions (see Fig. 8, bottom). The cavities are located systematically in the grooves. More and more cavities are identified within two large "main" grooves with increasing roller radii, and finally some new smaller grooves are detected besides the "main" grooves for the smallest roller radii, see Fig. 8, bottom. The large cavities of the emery ground surface with larger distances between each other are more important for the nucleation than the larger number of equally formed and distributed cavities on the fine sandblasted surface. Additionally, the active sites are more stable on the emery ground surface than on the fine sandblasted surfaces [29].

### 3.4. New results of the heating surfaces

The results according to standard of the newly treated heating elements are listed in detail in Table 5. Examples of 2D-profiles and of isometric representations of the topography are given in Figs. 10 and 11. The profiles show the typical enlargement of the ordinates over the abscissae with $z/x = 36$. The surfaces of the steel tube—the original and the gold plated one—are fine sandblasted with the same parameters as the surfaces

Table 5
Roughness parameters of heating elements according to DIN EN ISO 4287 (10.98) with the gauge length of $x = 0.5$ mm, without cut-off ($\lambda_c = \infty$)

| Heater element, Material | Treatment | | $P_a$ [µm] | $P_q$ [µm] | $P_p$ [µm] | $P_{\text{pm}}$ [µm] | $P_t$ [µm] | $P_z$ [µm] | runs |
|---|---|---|---|---|---|---|---|---|---|
| tube, $D = 15$ mm | fine sandblasted | average | 0.14 | 0.19 | 0.71 | 0.51 | 1.22 | 0.92 | 3219 |
| stainless steel | ($p_L = 1.5$ bar, $d_p = 25$ µm) | max. | 0.22 | 0.28 | 2.02 | 0.86 | 2.57 | 1.49 | |
| | | min. | 0.10 | 0.13 | 0.36 | 0.32 | 0.71 | 0.60 | |
| | | $\sigma$ | 0.02 | 0.03 | 0.17 | 0.07 | 0.24 | 0.15 | |
| | | $S_i$ [a] | 0.17 | 0.22 | 1.55 | | 2.52 | 2.21 | 4 |
| tube, $D = 15$ mm | fine sandblasted | average | 0.26 | 0.33 | 1.03 | 0.78 | 2.02 | 1.56 | 2159 |
| stainless steel | ($p_L = 1.5$ bar, $d_p = 25$ µm) | max. | 0.33 | 0.44 | 2.29 | 1.18 | 3.39 | 2.08 | |
| with a galvanically | | min. | 0.20 | 0.26 | 0.64 | 0.57 | 1.38 | 1.14 | |
| plated gold layer | | $\sigma$ | 0.02 | 0.03 | 0.21 | 0.08 | 0.28 | 0.14 | |
| | | $S_i$ [a] | 0.29 | 0.39 | 2.21 | | 4.03 | 3.56 | 4 |
| plate, $D = 35.0$ mm | manually polished | average | 0.11 | 0.14 | 0.46 | 0.28 | 0.88 | 0.56 | 873 |
| copper with a | emery paper (#1000 paper) | max. | 0.21 | 0.27 | 1.21 | 0.56 | 1.68 | 0.96 | |
| sputtered gold layer | | min. | 0.06 | 0.08 | 0.19 | 0.15 | 0.42 | 0.31 | |
| | | $\sigma$ | 0.03 | 0.03 | 0.15 | 0.06 | 0.19 | 0.09 | |
| | | $S_i$ [a] | 0.18 | 0.23 | 1.35 | | 2.57 | 2.22 | 1 |
| tube, $D = 25.0$ mm | fine sandblasted | average | 0.59 | 0.74 | 2.11 | 1.54 | 4.15 | 3.14 | 1225 |
| copper | ($p_L = 3$ bar) | max. | 0.78 | 1.00 | 4.41 | 2.40 | 6.79 | 4.26 | |
| | then medium sandblasted | min. | 0.41 | 0.51 | 1.26 | 1.00 | 2.67 | 1.99 | |
| | ($p_L = 1.5$ bar) | $\sigma$ | 0.07 | 0.09 | 0.43 | 0.21 | 0.61 | 0.41 | |
| | | $S_i$ [a] | 0.61 | 0.77 | 4.05 | | 7.24 | 6.69 | 2 |
| tube, $D = 25.0$ mm | fine sandblasted | average | 0.55 | 0.69 | 1.91 | 1.39 | 3.80 | 2.84 | 3169 |
| copper | ($p_L = 5$ bar) | max. | 0.74 | 0.97 | 5.21 | 2.14 | 7.53 | 3.99 | |
| | then medium sandblasted | min. | 0.36 | 0.44 | 0.99 | 0.82 | 2.36 | 1.82 | |
| | ($p_L = 1.5$ bar) | $\sigma$ | 0.07 | 0.08 | 0.38 | 0.21 | 0.57 | 0.38 | |
| | | $S_i$ [a] | 0.55 | 0.69 | 2.70 | | 6.60 | 4.82 | 4 |

[a] $S_i$ ($S_a$, $S_q$, $S_p$, $S_t$, $S_z$) correspond to the two-dimensional, see Table 3, the number of runs is the number of investigated topographies.

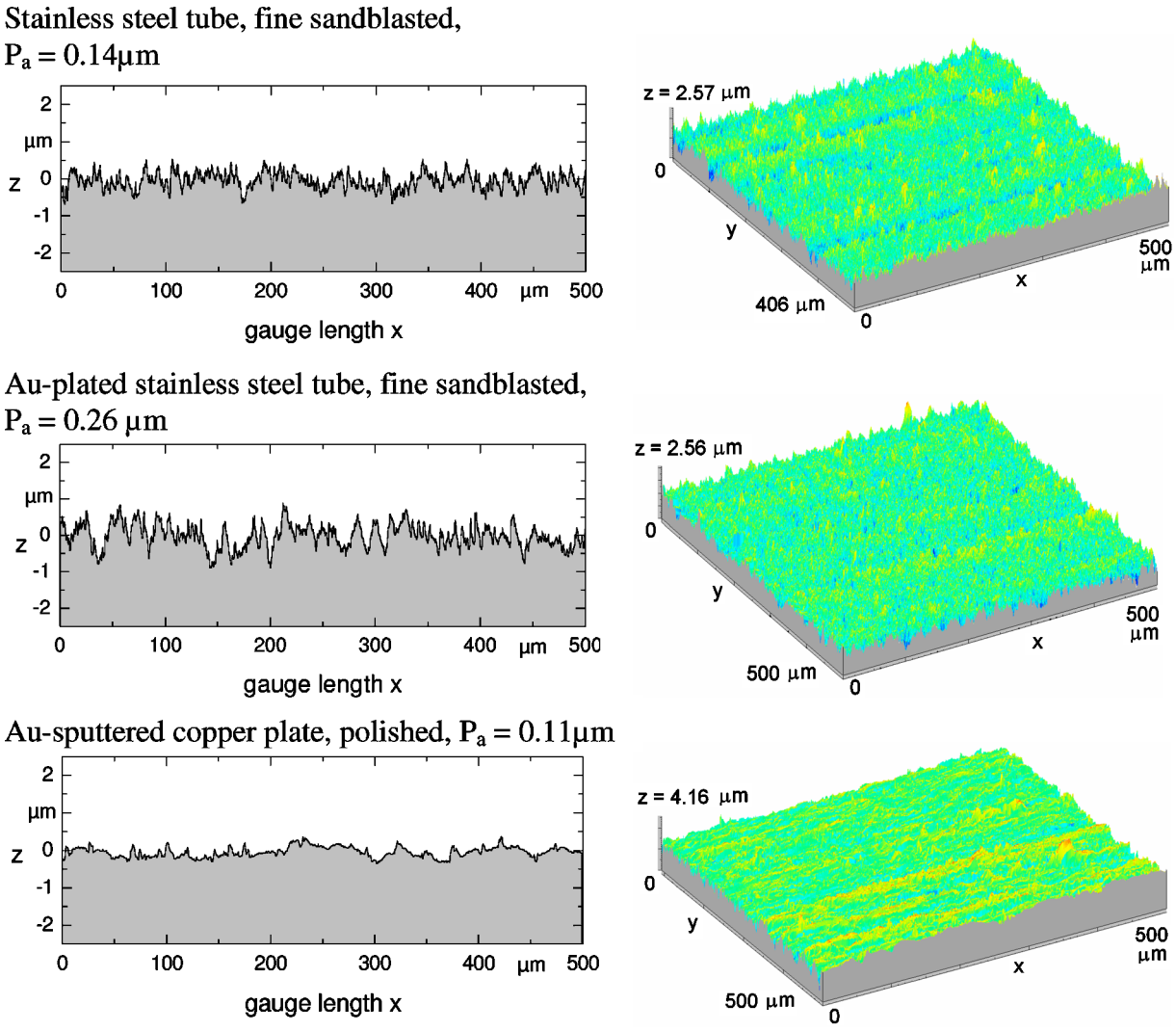


Fig. 10. Isometric (right) representation of the topography with one typical profile (left, enlargement $z/x = 36$) of the fine sandblasted stainless steel tube (original, top, gold-plated, middle) and the manually polished gold-sputtered copper plate (bottom).

in Table 4. The topographies of both surfaces are nearly identical, see Fig. 10, while the single profile and the averaged mean roughness (the $P_a$-values) are different, see Table 5. The results of the gold plated surface are similar to the other fine sandblasted surfaces—the copper tube and plate, the CuNi-tube. The profile in Fig. 10 is rather smooth compared to the gold plated copper tube [10]. The averaged $P_a$-value is 20% lower, cf. Tables 5 and 4. The differences may be explained by the larger number of runs considered in the case of the gold plated steel tube. The original steel tube is definitively smoother than the other fine sandblasted surfaces, see the profiles in Fig. 10 and the standardized roughness parameters in Table 5, although the surface is prepared by the same parameters. Single high peaks as in the case of the sputtered stainless steel layer on the copper plate cannot be observed (cf. also $P_p$ in Table 4 and [10]). The surface of the steel tube is similar to the fine sandblasted mild steel surface with $P_a = 0.16$ µm [20]. The same holds for other fine sandblasted steel tubes and sheets [22].

The gold sputtered copper plate [9] is manually polished, see Table 4, bottom. Surface structure and $P_a$-values are similar to those of the Ni-plated surface, cf. Tables 4 and 5. Differences in the boiling curves resulting from the heat transfer measurements [9,12,23] may be deduced to the different wettability of the gold and the Nickel-layer.

The copper tube with $D = 25.4$ mm is fine sandblasted and then rolled [10]. The macro cavities are removed. The flattening procedure was slightly varied to obtain more reentrant macrocavities. The outer diameter is slightly reduced due to the different surface preparations [11]. The copper tube of $D = 25$ mm is then sandblasted by different methods succeeding each other, fine then medium, see Table 2 and for the roughness parameters, see Table 5. By this, a surface micro structure more representative to industrial ones with higher roughness values and some reentrant cavities due to the drawing process is provided (as applied for evaporator tubes). The surface roughness is considerably higher and the surface is not as regular as the fine sandblasted one, cf. Figs. 11 and 10. In the first instance, the surface is fine sandblasted by a higher pressure with $p_L = 3$ bar and a particle fraction ($d_p = 0.2 \ldots 0.3$ mm), and then prepared by a fraction of larger particle sizes ($d_p = 0.5 \ldots 0.8$ mm) with

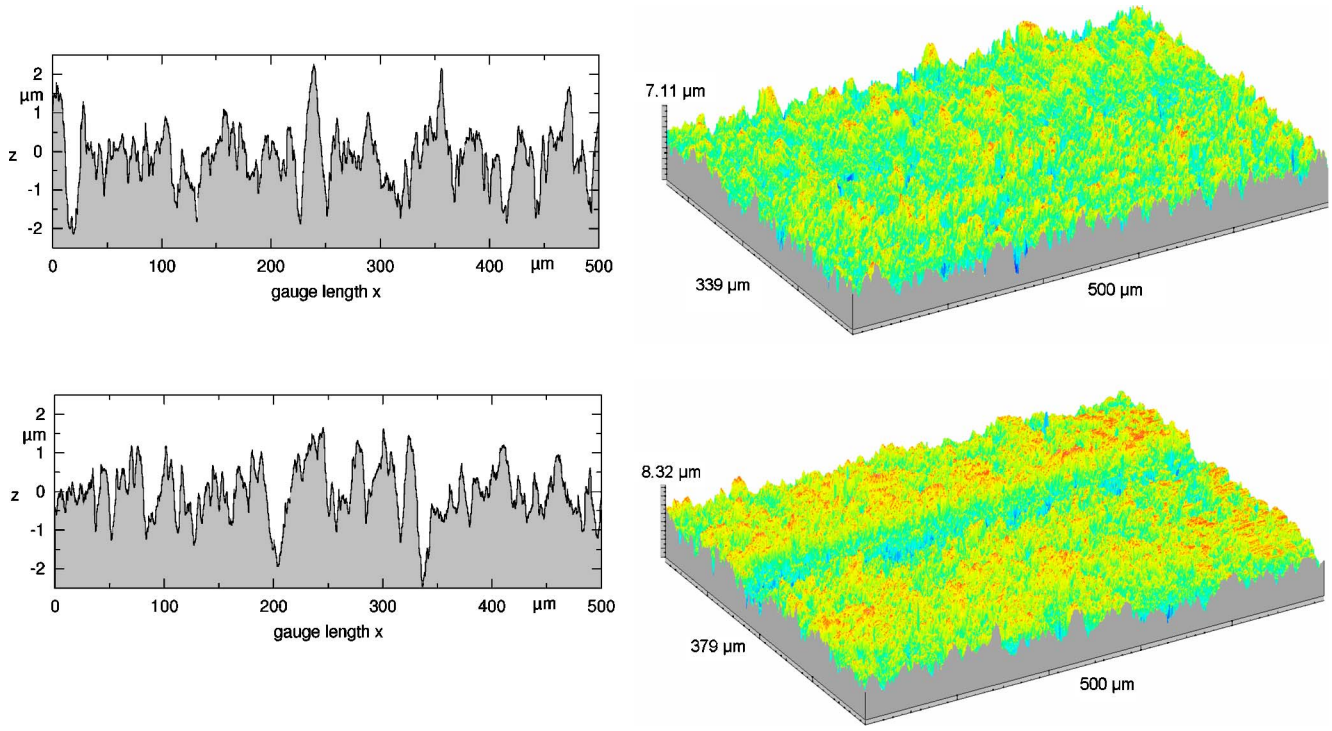


Fig. 11. Isometric representation of the topography (right) with one typical profile (enlargement $z/x = 36$, left) of the copper tube sandblasted by two succeeding steps: fine ($p_L = 3$ bar, top of Fig. 11, and 5 bar, bottom of Fig. 11) and medium ($p_L = 1.5$ bar both).

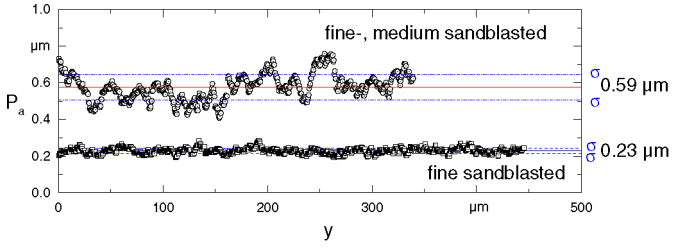


Fig. 12. $P_a$ of each scan of one measured topography of the fine sandblasted copper tube ($p_L = 1.5$ bar) and of the fine ($p_L = 3.0$ bar) and subsequently medium sandblasted ($p_L = 1.5$ bar) tube.

a lower pressure $p_L = 1.5$ bar (before the rolling procedure). The pressure is increased in the fine sandblasting procedure after the removal of the macro cavities. The two surfaces show the highest $P_a$-values and especially $P_t$ and $P_z$-values for all surfaces investigated in this project due to the larger sizes of the grains ($d_p = 50$–$80$ µm). The values of the surface prepared by the higher pressure are smaller than those of the surface prepared by the lower pressure, but the differences are within the experimental scatter, see Fig. 12.

The number of runs, i.e. the number of profiles investigated in the past were often restricted between 10 and in maximum 50 [20]. In Table 5, all measured profiles are considered, also those of the topographies. The $P_a$-values of each scan of the topography of the first fine then medium sandblasted surface are plotted as function of $y$ in Fig. 12 to visualize the differences in $P_a$-values of the different profiles. $P_a$-values scatters from near the reference $P_a = 0.4$ µm to 0.8 µm, smoother parts change to rougher ones within small distances. The heat transfer coefficient would scatter locally of ca. 7.5% according to

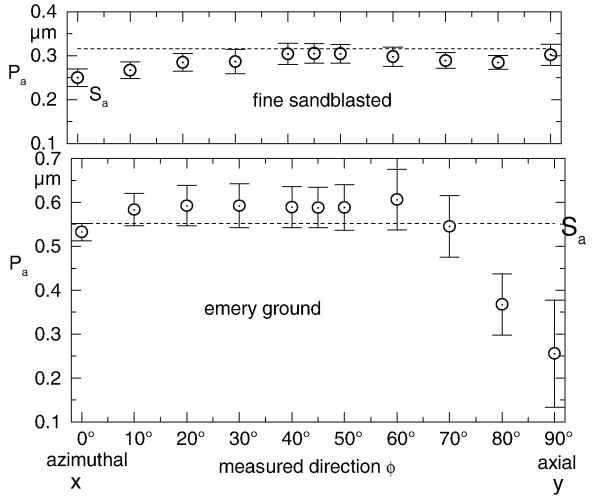


Fig. 13. $P_a$ as function of the measuring direction ($x$ = azimuthal, $y$ = axial) for the fine sandblasted copper surface and the emery ground tube of Fig. 8.

the VDI-Heat Atlas [1]. It is obvious that the number of runs of such irregular surfaces have to be higher than for the regular fine sandblasted ones to receive representative information, cf. Fig. 12.

The standardized roughness parameters result from the manufacturing process and are used for the empirical correlation for the heat transfer. The two-dimensional profiles have to be measured in the direction of the main roughness according to the standard, e.g. for emery ground surfaces in normal direction to the grooves. The real three-dimensional surface is smoother, see the $S_a$-value and the $P_a$-value as function of the measured direction to the grooves in Fig. 13 (0° = normal to the grooves

in $x$-direction and 90° = along the grooves in $y$-direction). The $P_a$-values in $x$-direction are twice as high as the values of $P_a$ in $y$-direction for the deterministic structures. In contrary, the parameters of the uniform fine sandblasted surface (Fig. 13, top) are independent of the measuring direction. $S_a$ is higher than $P_a$, because waviness superimposes the very fine microstructure.

Previous results of the statistical analysis are represented in Fig. 14 in form of the total number of potential sites as function of the roller radii for the fine sandblasted surface of Fig. 6 and the two variations of the fine-medium sandblasted ones. The number of cavities is higher on the fine sandblasted surface, while the total number of cavities $N/A_{\text{pot}}$ on the fine-medium sandblasted surfaces are nearly the same for all roller radii except for the largest one. The size distribution for the smooth and the rough surface is demonstrated in Fig. 15 in form of a density distribution of $P5^*$. The sizes of the cavities are regularly distributed in both cases, but the distribution of the fine-medium sandblasted surface is wider than that of the fine sandblasted surface. The surface shows two times more large cavities as the fine sandblasted one, favourite for the beginning nucleation and for stable bubble nuclei.

The results of the third rolling procedure after the first fine-medium sandblasting are shown in Fig. 16 and details of the macro cavities in Fig. 17. The once rolled "secondary" structure shows open macro cavities regularly distributed on the tube surface of ca. 120 × 250 × 50 µm with the long side of the cavity in $y$-direction (in the tube axe), see the top view of the measured topography in Fig. 16, right. The colours in the original representation (or the grey levels in the case of the lack of colours) indicate the quantitative $z$-data (bottom = dark blue or dark grey, see the scale in Fig. 16, left). The gauge length in $x$-direction is twice as long as for the microstructure in Figs. 10 and 11 to have some representative macro cavities. The resolution is $\Delta x = \Delta y = 0.5$ mm. A larger topography is provided with lower resolution in $y$-direction in [10,15]. The macro cavities are equally distributed in azimuthal direction as shown in [10,11]. The "main" structure is produced by a second procedure where the material is flattened into the cavities. The macro cavities become very narrow, especially in the middle, see Fig. 16, left, and Fig. 17, top (possible misinterpretation at the edges by the stylus tip has to be considered). The different crest profiles visualized by the detail of the cavity in Fig. 17 result from the flattening tool and could be reproduced in constant distance, see the "stripes" within the topography in Fig. 16, left. The profiles in Fig. 18 demonstrate again the original deep rolled macro cavities. The mouth width becomes smaller, the total depth is reduced to values of ca. 15 µm and the material between the macro cavities is really flattened after the second procedure.

In the following the microstructure on the different locations —between the rows of cavities, between the cavities themselves and at the bottom of the cavities—is analysed precisely by looking on the details of the topographies and the calculated roughness parameters for the secondary and main structure in Fig. 19 and Table 6. The gauge length and the enlargement of the topographies differ significantly. The gauge length of

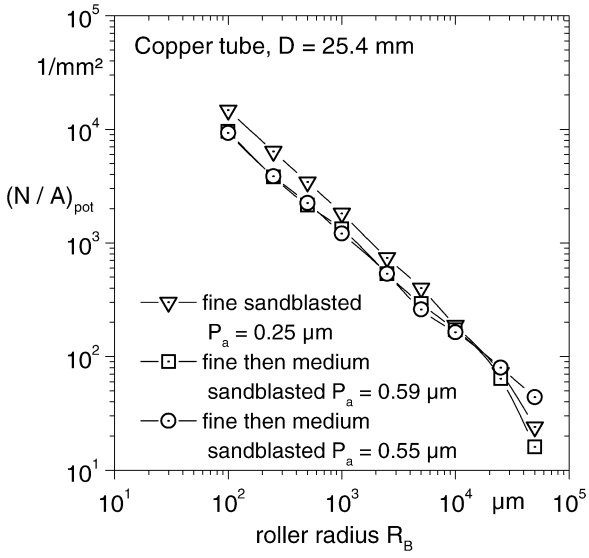


Fig. 14. Total number of potential sites $N/A_{\text{pot}}$ of differently sandblasted copper tube as function of the roller radius $R_B$.

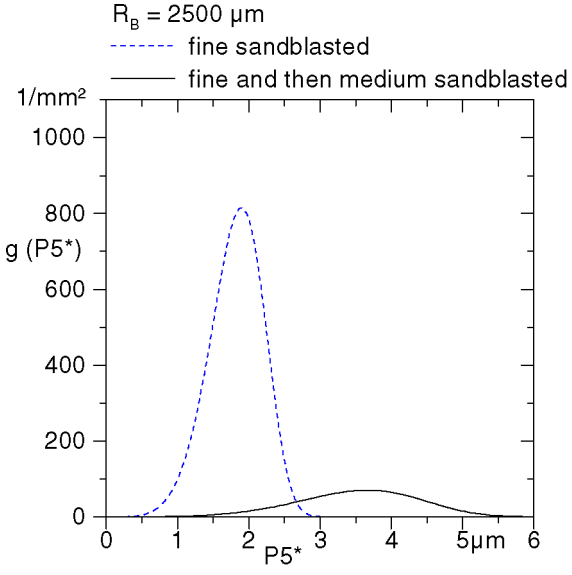


Fig. 15. Density distribution of $P5^*$ for the three-dimensional analysis for $R_B = 2500$ µm for the fine sandblasted surface with $P_a = 0.25$ µm and the fine and medium sandblasted surface with $P_a = 0.59$ µm.

$x = 0.5$ mm could only be realized between two rows of cavities, see Fig. 19, top, so that this value may be directly compared to the other microstructures investigated (Tables 4 and 5).

The previous fine- and medium sandblasted microstructure between the macro cavities is almost preserved by the rolling procedure, see the detail of the macro cavity in Fig. 17, bottom, and Fig. 19, left. The higher average $P_a$-value ($P_a = 0.65$ µm) lies within the upper experimental scatter of Fig. 12. The previous microstructure becomes somewhat smoother between two macro cavities, because it is slightly influenced by the rolling tool.

The fine-medium sandblasted microstructure within the cavities vanishes completely after the rolling and the flattening procedure, cf. the bottom in Fig. 17. The mean roughness values

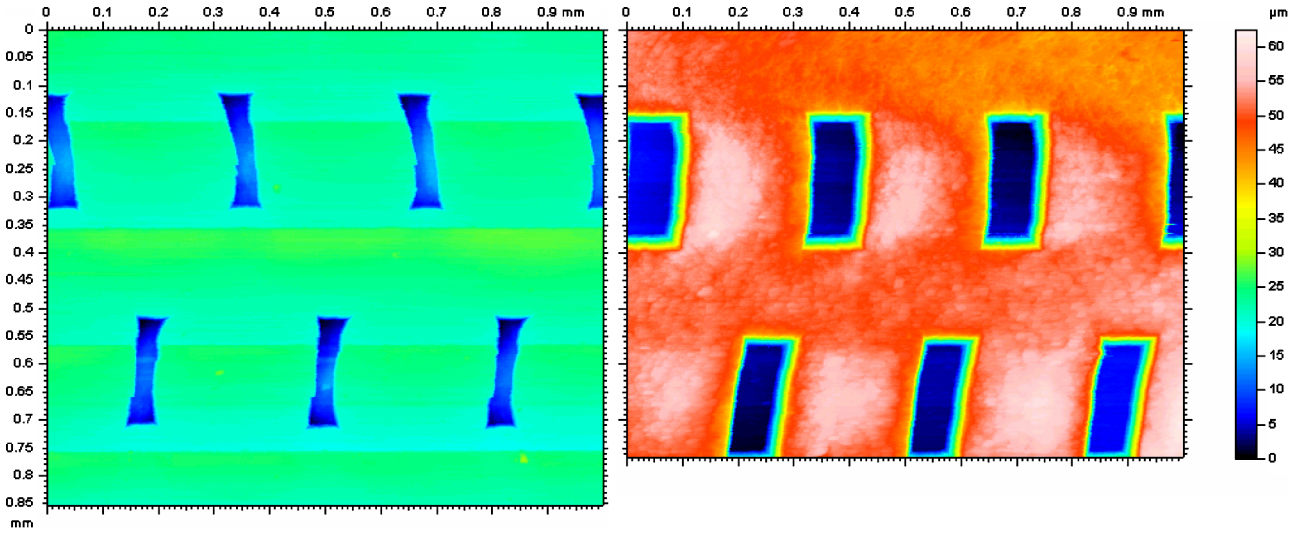


Fig. 16. Top view of the rolled macro cavities within the topography of the copper tube ($D = 25.0$) with fine- and medium sandblasted microstructure (cf. also [11]): Left: main structure, once rolled and subsequently flattened. Right: secondary structure, once rolled.

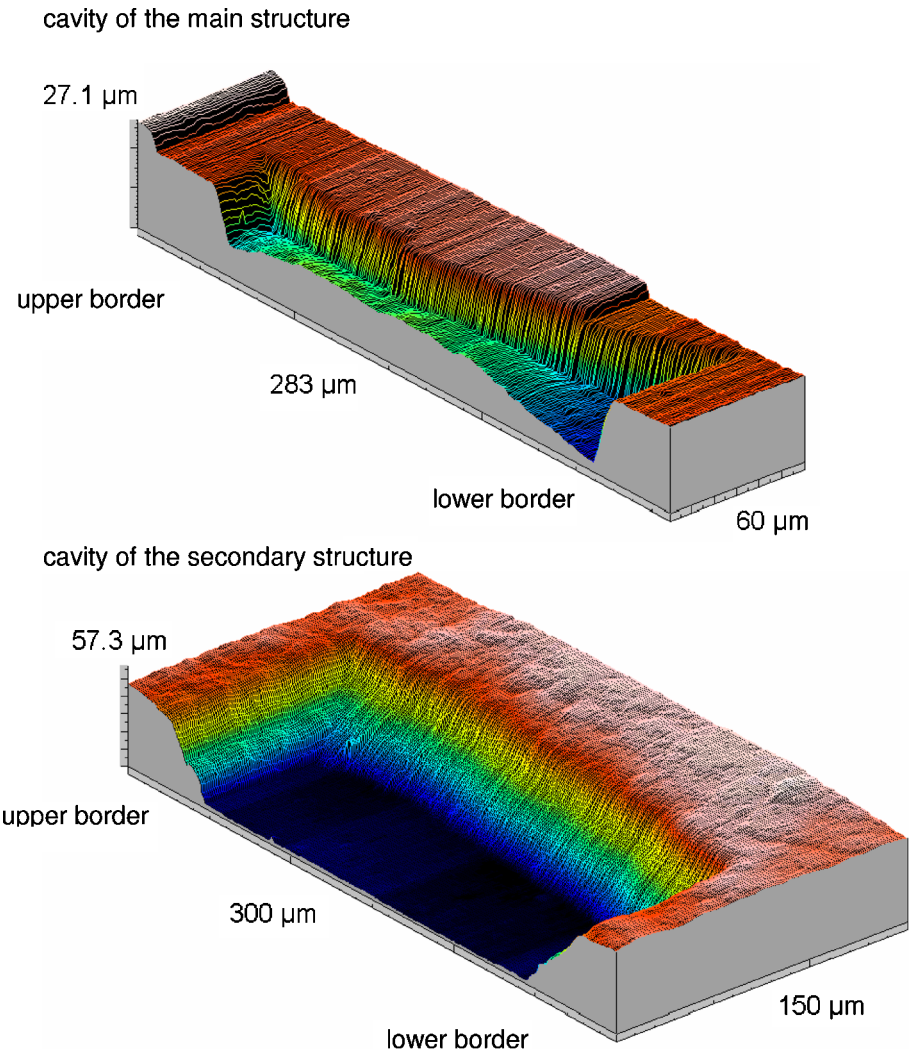


Fig. 17. Isometric representation of a longitudinal section of the rolled macro cavities within the topography of the copper tube ($D = 25.0$) with fine- and medium sandblasted microstructure (cf. also [11]): Top: main structure, once rolled and subsequently flattened. Bottom: secondary structure, once rolled.

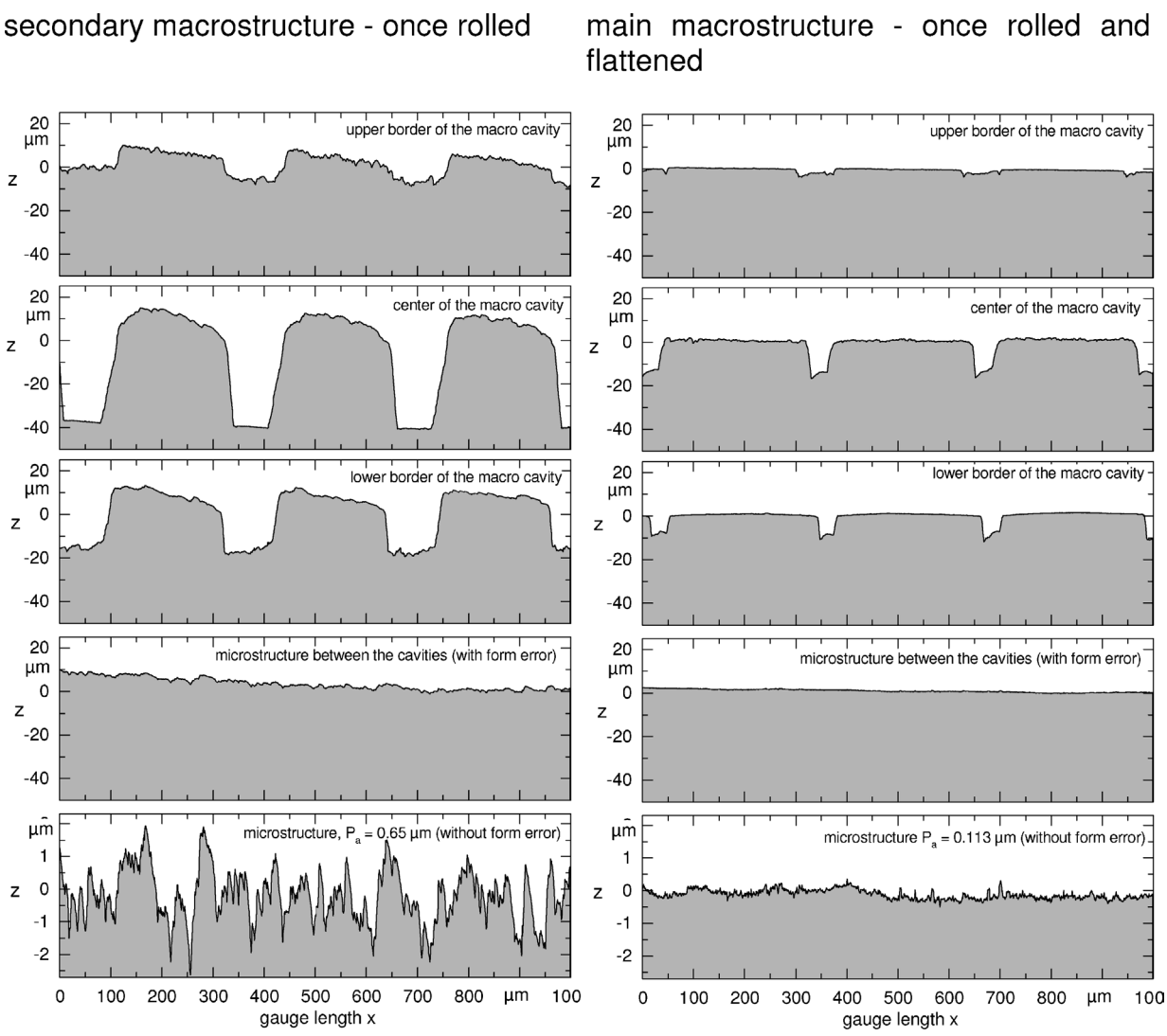


Fig. 18. Profiles of the upper and lower border, and center of the macro cavities within the topography of the copper tube ($D = 25.0$) with fine- and medium sandblasted microstructure (cf. also [11]): Right: main structure, once rolled and subsequently flattened. Left: secondary structure, once rolled.

of the flattened microstructure are similar to the polished ones, see Tables 6 and 4. The higher values within the bottom of the macro cavities of the main structure are due to the short gauge length and edge fringing. The new microstructure between the macro-cavities of the main structure is discussed intensively in [11] in this issue by means of the profiles belonging to the topographies in Fig. 19, right. The crest profiles—two or three succeeding profiles—may act as potential nucleation sites.

It is possible to separate the influence of macrostructure and microstructure by this method, i.e. the analysis of the macro cavities themself and in addition the look on the details. This is important following the results of heat transfer and bubble formation on the same surface with and without macro cavities in boiling R134a, 2-Propanol and Propane [11]. The next step may be the preparation of a "flattened" microstructure as in Fig. 18, right, without reentrant macro cavities. The standardized roughness parameters and one topography of first roughness measurements are represented in the paper of the other subproject [11] showing a similar $P_a$-value and microstructure with crest profile as in Fig. 19, right.

## 4. Conclusion

The heating elements of the research groups interior the joint project on fundamentals of boiling heat transfer are prepared by special reproducible processes in the laboratory in such a way, that the microstructure are comparable to those used in industry. Most of the surfaces are fine sandblasted with corundum grain of a small size distribution with low pressure. Some surfaces are manually polished due to the sensible measurement technique and one tube is emery ground to compare the heat transfer and bubble formation with former ones. New three-dimensional contactless measurement techniques are used to get detailed information about the heated surface and its cavities. The analysis of the microstructure implies two-dimensional profiles and three dimensional topographies.

The results of the roughness measurements are summarized as follows: The fine sandblasting treatment results in a granular diffuse surface microstructure with an average mean roughness parameter of $P_a = 0.25\ \mu\text{m} \pm 0.05\ \mu\text{m}$. The roughness parameters becomes smaller for harder material as stainless steel.

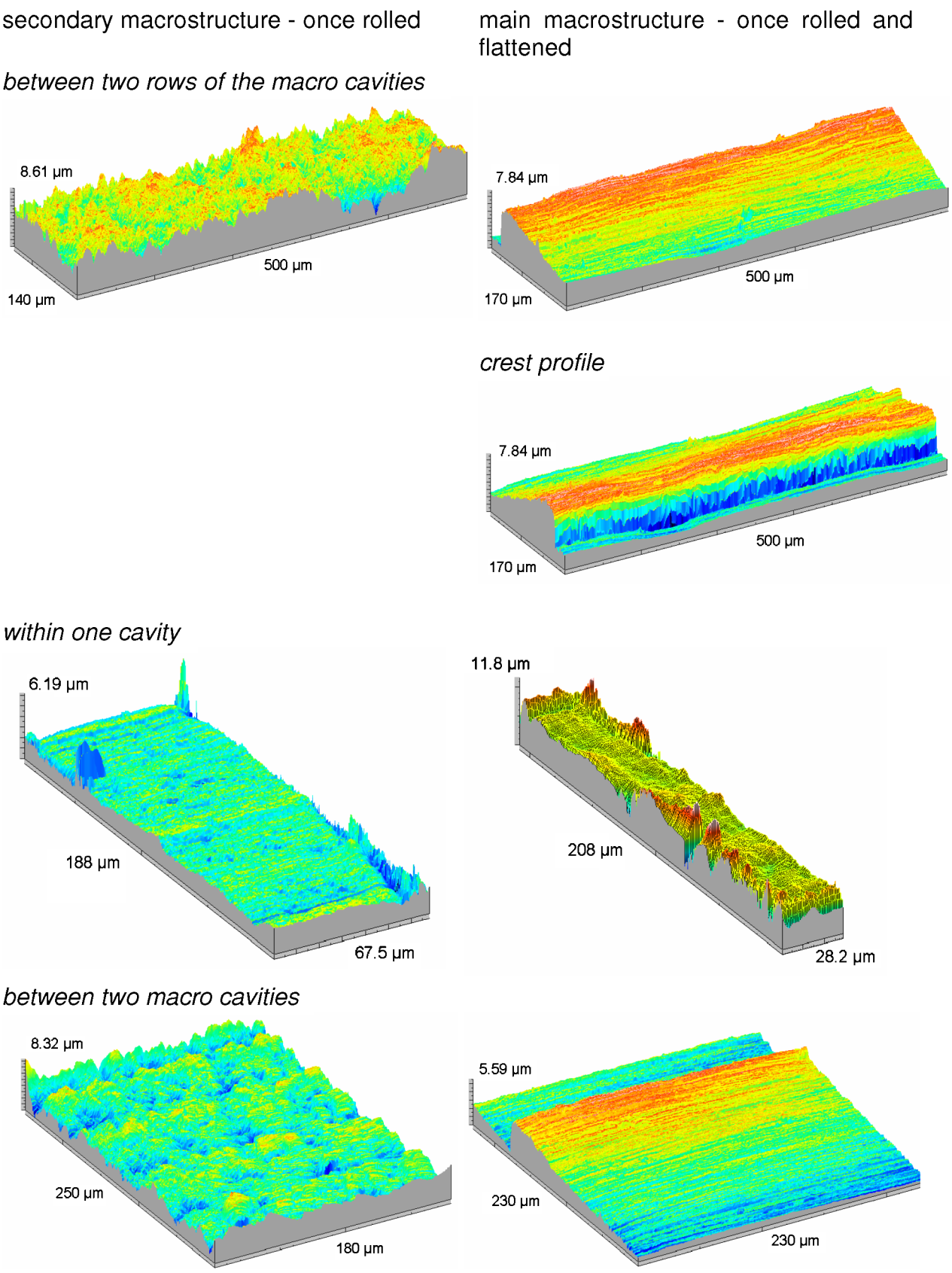


Fig. 19. Isometric representation of details of the microstructure after the rolling process on the copper tube ($D = 25.0$) with previously fine- and medium sandblasted microstructure (cf. also [11]): Right: main structure, once rolled and subsequently flattened. Left: secondary structure, once rolled.

Table 6
Roughness parameters of the microstructure within and between the macro cavities on the copper tube with $D = 25.0$ mm according to DIN EN ISO 4287 (10.98) with different gauge lengths, without cut-off ($\lambda_c = \infty$)

| Heater element, Material Treatment | Location of measurement | | $P_a$ [μm] | $P_q$ [μm] | $P_p$ [μm] | $P_{pm}$ [μm] | $P_t$ [μm] | $P_z$ [μm] | runs | gauge length [mm] |
|---|---|---|---|---|---|---|---|---|---|---|
| tube, $D = 25.0$ mm copper main structure: rolled and flattened | between two rows of cavities | average | 0.14 | 0.17 | 0.58 | 0.32 | 1.04 | 0.59 | 341 | 0.5 |
| | | max. | 0.70 | 0.84 | 2.90 | 1.90 | 4.34 | 3.20 | | |
| | | min. | 0.07 | 0.08 | 0.26 | 0.16 | 0.51 | 0.32 | | |
| | | $\sigma$ | 0.06 | 0.08 | 0.35 | 0.19 | 0.50 | 0.32 | | |
| | between two rows of cavities | average | 0.12 | 0.15 | 0.62 | 0.31 | 1.02 | 0.56 | 341 | 0.5 |
| | | max. | 0.68 | 0.87 | 2.85 | 1.73 | 4.21 | 2.93 | | |
| | | min. | 0.04 | 0.05 | 0.17 | 0.13 | 0.38 | 0.26 | | |
| | | $\sigma$ | 0.07 | 0.09 | 0.45 | 0.17 | 0.54 | 0.29 | | |
| | within one cavity | average | 0.46 | 0.60 | 1.30 | 0.53 | 2.85 | 1.12 | 417 | 0.028 |
| | | max. | 1.29 | 1.67 | 4.12 | 1.68 | 6.79 | 3.18 | | |
| | | min. | 0.14 | 0.19 | 0.28 | 0.16 | 0.83 | 0.46 | | |
| | | $\sigma$ | 0.19 | 0.24 | 0.61 | 0.22 | 1.08 | 0.39 | | |
| | between two cavities | average | 0.06 | 0.08 | 0.28 | 0.16 | 0.50 | 0.29 | 461 | 0.23 |
| | | max. | 0.37 | 0.50 | 1.55 | 1.13 | 2.72 | 1.55 | | |
| | | min. | 0.03 | 0.04 | 0.11 | 0.09 | 0.24 | 0.16 | | |
| | | $\sigma$ | 0.03 | 0.04 | 0.15 | 0.08 | 0.23 | 0.12 | | |
| tube, $D = 25.0$ mm copper secondary structure: once rolled | between two rows of macro cavities | average | 0.64 | 0.81 | 2.41 | 1.77 | 4.92 | 3.69 | 281 | 1.0 |
| | | max. | 1.13 | 1.41 | 3.98 | 2.64 | 8.49 | 5.36 | | |
| | | min. | 0.53 | 0.67 | 1.47 | 1.29 | 3.62 | 3.00 | | |
| | | $\sigma$ | 0.09 | 0.12 | 0.46 | 0.23 | 0.76 | 0.46 | | |
| | between two cavities | average | 0.45 | 0.56 | 1.26 | 0.83 | 2.74 | 1.80 | 500 | 0.18 |
| | | max. | 0.79 | 1.00 | 3.16 | 1.66 | 4.99 | 3.04 | | |
| | | min. | 0.26 | 0.34 | 0.62 | 0.43 | 1.55 | 1.06 | | |
| | | $\sigma$ | 0.09 | 0.12 | 0.41 | 0.22 | 0.55 | 0.41 | | |
| | within one cavity | average | 0.14 | 0.21 | 0.75 | 0.29 | 1.43 | 0.58 | 401 | 0.07 |
| | | max. | 0.81 | 1.41 | 8.41 | 1.75 | 9.92 | 2.90 | | |
| | | min. | 0.06 | 0.07 | 0.16 | 0.11 | 0.37 | 0.23 | | |
| | | $\sigma$ | 0.10 | 0.14 | 0.69 | 0.20 | 0.88 | 0.31 | | |

The parameters of surface treatment have to be adjusted to the hardness of the material to obtain the same microstructure. Two succeeding procedures of sandblasting are carried out aiming at a rougher, more technical surface ($P_a \approx 0.55$ μm). The number of measurements runs should be increased for more irregular rougher surfaces as the fine-medium sandblasted one to obtain representative mean roughness values.

A first quantitative description of the surfaces may be received by the standardized roughness parameter. The bubble formation may be related to the surface structures characterized quantitatively by special calculation methods to receive the local distribution of the cavities and their size distribution. The method of the envelope area for topographies is used to determine the actual $x$–$y$-location and size of the cavities on the surface. The fine and the fine-medium sandblasted surfaces have nearly the same total number of potential nucleation sites, but the size distributions are different. The fine sandblasted surface has a lot of stochastically distributed cavities with similar small sizes, while the rougher surface offers both, large and small cavities. The large ones are the favourable ones for beginning nucleation and for stable bubble nuclei.

The microstructure is preserved after a first rolling procedure providing macro cavities. A following flattening procedure aiming at reentrant macro cavities destroys the previous microstructure. The result is a surface as smooth as if it is polished. The microstructure between and within the macro cavities can be characterized quantitatively as the other surfaces without superimposed macrostructure.

## Acknowledgements

The author highly appreciates financial support of the Deutsche Forschungsgemeinschaft (DFG) in the frame of a joint research project on fundamentals of boiling heat transfer. The author thanks all participants of the joint research project for helpful discussions and the Wieland Werke, Ulm, Germany, for the precise preparation of the macro cavities on the tube surfaces.

## References

[1] D. Gorenflo, Behältersieden; Abschnitt Hab; VDI-Wärmeatlas, ninth ed., Springer, Berlin, 2002. Cf also: Pool boiling, Chapt. Ha, VDI-Heat Atlas, VDI, Düsseldorf, 1993.

[2] M.G. Cooper, Heat flow rates in saturated nucleate pool boiling—a wide ranging examination using reduced properties, Adv. Heat Transfer 16 (1984) 157–239.

[3] G. Barthau, E. Hahne, Nucleation site density and heat transfer in nucleate pool boiling of refrigerant R134a in a wide pressure range, in: Proc. 3rd European Thermal Sci. Conf. Heidelberg, Germany, 2000, vol. 2, pp. 731–736.
[4] G. Barthau, E. Hahne, Experimental study of nucleate pool boiling of R134a on a stainless steel tube, in: Proc. 5th Int. Conf. on Boiling Heat Transfer, Montego Bay, Jamaica, 2003.
[5] D. Gorenflo, W. Fust, A. Luke, E. Danger, U. Chandra, Pool boiling heat transfer from tubes with basic surface modifications for enhancement—Design of the test tubes and first measurements, in: Proc. 3rd European Thermal Sci. Conf. Heidelberg, Germany, 2000, vol. 2, pp. 743–748.
[6] D. Gorenflo, E. Danger, A. Luke, S. Kotthoff, U. Chandra, C. Ranganayakulu, Bubble formation with pool boiling on tubes with and without basic modifications for enhancement, in: Proc. 5th Int. Conf. on Boiling Heat Transfer, Montego Bay, Jamaika, 2003.
[7] R. Maurus, V. Ilchenko, T. Sattelmayer, Study of the bubble characteristics and the local void fraction in subcooled flow boiling using digital imaging—and analysing techniques, in: Proc. 5th World Conference on Experimental Heat Transfer, Fluid Mechanics and Thermodynamics, Thessaloniki, Greece, 2001, vol. 2, pp. 1329–1336.
[8] G. Barthau, E. Hahne, Nucleate pool boiling of R134a on a gold-plated copper test tube, in: Proc. Int. Inst. Refrig. Conf., Comm B1 2001/5, Paderborn, Germany, 2001, pp. 372–379.
[9] M. Buchholz, H. Auracher, T. Lüttich, W. Marquardt, A study of local heat transfer mechanisms along the entire boiling curve by means of microsensors, Int. J. Thermal Sci. 45 (3) (2006) 269–283 (this issue).
[10] A. Luke, D. Gorenflo, Roughness of evaporator surfaces for joint research project and development of a database for roughness bubble formation and heat transfer, in: Proc. Int. Inst. Refrig. Conf., Comm B1 2001/5, Paderborn, Germany, 2001, pp. 362–371.
[11] S. Kotthoff, D. Gorenflo, E. Danger, A. Luke, Heat transfer and bubble formation for pool boiling on tubes with basic surface modifications for enhancement, Int. J. Thermal Sci. 45 (3) (2006) 217–236 (this issue).
[12] M. Buchholz, T. Lüttich, H. Auracher, W. Marquardt, Steady state pool boiling experiments with water between nucleate and film boiling, in: Proc. 3rd. European Thermal Sci. Conf., Heidelberg, Germany, 2000, vol. 2, pp. 761–766.
[13] A. Luke, New methods of characterization for the microstructure of heated surfaces in boiling, in: Proc. 3rd. European Thermal Sci. Conf., Heidelberg, Germany, 2000, vol. 2, pp. 737–742.
[14] E. Danger, U. Chandra, A. Beutler, D. Gorenflo, Basic surface modifications for enhancement of pool boiling heat transfer, in: Proc. Int. Inst. Refrig. Conf., Comm B1 2001/5, Paderborn, Germany, 2001, pp. 380–387.
[15] A. Luke, Thermo- and fluiddynamic in boiling—Connection between surface roughness, bubble formation and heat transfer, in: Proc. 5th Int. Conf. on Boiling Heat Transfer, Montego Bay, Jamaica, 2003.
[16] K. Shi, E. Hahne, U. Groß, Pool boiling heat transfer in HFC-134a, HFC-152a and their mixtures, in: Proc. XVIIIth Int. Congr. of Refrig., Montreal, Canada, 1991, vol. II, pp. 459–463.
[17] R. Mertz, M. Groll, Evaporation heat transfer from enhanced industrial heat exchanger tubes using hydrocarbons, Heat and Technol. 17 (2) (1999) 3–11.
[18] D. Gorenflo, P. Sokol, S. Caplanis, Zum Wärmeübergang beim Blasensieden von Kohlenwasserstoffen und Halogen-Kältemitteln an einem Glattrohr und einem Hochleistungs-Rippenrohr, Wärme- und Stoffübertragung 26 (1991) 273–281.
[19] D.B.R. Kenning, T. Kono, M. Wienecke, Investigation of boiling heat transfer by liquid crystal thermography, in: Proc. ASME—ZSITS Int. Thermal Sci. Seminar, Bled, Slovenia, 2000, pp. 35–46.
[20] A. Luke, Pool boiling heat transfer from horizontal tubes with different surface roughness, Int. J. Refrig. 20 (8) (1997) 561–574, cf. also A. Luke, Beitrag zum Einfluß der Mikrostruktur auf den Wärmeübergang beim Blasensieden, Diss. Universität, GH, Paderborn, 1996.
[21] D. Gorenflo, W. Fath, Heat transfer at pool boiling outside of finned tubes at high saturation pressures, in Proc. XVIIth Int. Congr. Refrig. Wien 1987, vol. B, pp. 955–960.
[22] A. Luke, Active and potential bubble nucleation sites on different structured heated surfaces, Chem. Engrg. Res. Design 82 (2004) 462–470.
[23] M. Buchholz, T. Lüttich, H. Auracher, W. Marquardt, Experimental investigation of local processes in pool boiling along the entire boiling curve, Internat. J. Heat Fluid Flow 25 (2004) 243–261.
[24] R. Hohl, J. Blum, M. Buchholz, T. Lüttich, H. Auracher, W. Marquardt, Boiling experiments under steady state and controlled transient conditions, in: Proc. “Boiling 2000: Phenomena & Emerging Applications” Conf., Anchorage, USA, 2000, vol. 1, pp. 236–252.
[25] K. Spindler, P. Englisch, E. Hahne, Vergleich des Wärmeübergangs beim Behältersieden von R404A mit R22 an einem feinsandgestrahlten Kupferrohr und einem Hochleistungsrohr, DKV-Tagungsbericht, Bd. II. 1 24 (1997) 150–168.
[26] P. Hübner, D. Gorenflo, A. Luke, Circumferential temperature distributions on plain and finned tubes in pool boiling, in: Proc. 3rd Conf. Compact Heat Exchangers, Davos, Switzerland, 2001, pp. 383–390.
[27] E. Hahne, G. Barthau, Heat transfer and nucleation in pool-boiling, Int. J. Thermal Sci. 45 (3) (2006) 209–216 (this issue).
[28] R. Maurus, K. Hermanson, T. Sattelmayer, Measurements of the bubble behaviour and the phase boundary velocity in subcooled flow boiling, in: Proc. 3rd European Thermal Sci. Conference, Heidelberg, Germany, 2000, vol.2, pp. 719–724.
[29] A. Luke, E. Danger, D. Gorenflo, Size distributions of active and potential sites in pool boiling, in: Proc. 12th Int. Heat Transfer Conf., Grenoble, France, 2002, vol. 3, pp. 383–388.
[30] A. Luke, E. Danger, Size distribution of active and potential nucleation sites on horizontal evaporator tubes, in: Proc. Int. Inst. Refrig. Comm. B1 Conf. 2001/5, Paderborn, Germany, 2001, pp. 396–403.
[31] A. Luke, E. Baumhögger, P. Scheunemann, 3-dimensional description of the microstructure of heated surfaces in nucleate pool boiling, Multiphase Sci. Technol. 12 (2) (2001) 1–13.
[32] K. Bier, D. Gorenflo, M.I. Salem, Y.M. Tanes, Pool boiling heat transfer and size of active nucleation centers for horizontal plates with different surface roughness, in: Proc. 6th Int. Heat Transfer Conf., Toronto, Canada, 1978, vol. 1, pp. 151–156.
[33] G. Goch, P. Lehmann, Contactless topography and microhardness measurements using scanning near-field acoustic microscopy (SNAM), in: Euspen, Bremen, Germany, 1999, pp. 479–482.
[34] K.J. Stout, P.J. Sullivan, W.P. Dong, E. Mainsah, N. Luo, H. Zahouani, The development of methods for the characterisation of roughness in three dimensions, in: Publ. No. EUR 15178 EN, 1993.
[35] K. Stephan, Beitrag zur Thermodynamik des Wärmeüberganges beim Sieden, Abhandlung des D. Kältetech. Vereins, vol. 18, C.F. Müller-Verlag, Karlsruhe, 1964.